Glutamatergic Supramammillary Nucleus Neurons Promote Active Coping to Stress

Salli-Ann Holloway[1], Megan Votoupal[2], Abraham Escobedo[1], Alex A. Legaria [3,4], Imeh Ndiokho[5], Tasheia Floyd[6], Alexxai V. Kravitz [1,3,4], Michael R. Bruchas[7,8,9,10, *], Aaron J. Norris[1*]

Affiliations:

1 Department of Anesthesiology, Washington University in St. Louis, St. Louis, MO

2 Department of Medicine, Northwestern University Feinberg School of Medicine, Chicago IL

3 Department of Neuroscience, Washington University in St. Louis, St. Louis, MO

4 Department of Psychiatry, Washington University in St. Louis, St. Louis, MO

5 Medical College of Wisconsin, Milwaukee WI

6 Department of Obstetrics and Gynecology, Washington University in St. Louis, St. Louis, MO

7 Center for Neurobiology of Addiction, Pain, and Emotion University of Washington, Seattle, WA

8 Department of Anesthesiology and Pain Medicine University of Washington, Seattle, WA

9 Department of Pharmacology University of Washington, Seattle, WA

10 Department of Bioengineering University of Washington, Seattle, WA

* Corresponding authors

Lead Contact:

Aaron Norris

660 S. Euclid Ave, CSRB 5536

Saint Louis, MO 63110

norris@wustl.edu

(314)273-4422

Abstract

Threat-response neural circuits are conserved across species and have roles in normal behaviors and psychiatric diseases. Maladaptive changes in these neural circuits contribute to stress, mood, and anxiety disorders. Active coping in response to stressors is psychosocial factor associated with resilience against stress induced mood and anxiety disorders. The neural circuitry underlying active coping is poorly understood but the functioning of these circuits could be key for overcoming anxiety and related disorders. The supramammillary nucleus (SuM) has been suggested to be engaged by threat and found to have efferent connections to stress-sensitive brain regions. We identified a unique population of glutamatergic SuM neurons that project to the POA. Using

retrograde adeno associated viral (AAV) and combinatorial genetic tools we delineated the extensive arborization of these cells, identifying projections to brain nodes which mediate various features of the stress and threat response including the paraventricular nucleus (PV), periaqueductal gray (PAG), and the habenula (Hb). Here we report that the POA projecting subset of SuM neurons are activated by acute threatening stressors, based on fiber photometry measurements. We found that selective photoactivation of the target SuM population drives aversive and active coping behaviors. Furthermore, activation of these SuM neurons is sufficient to convert passive coping strategies to active behaviors. These findings indicate new circuit mechanisms which governs state transitions between active and passive responses to stress offering opportunities for furthering our neurobiological understanding of stress while helping to identify putative treatments for common psychiatric conditions.

Introduction

Threat-response neural circuits are conserved across species and have roles in normal behaviors and psychiatric diseases(1-4). Maladaptive changes in these neural circuits contribute to stress, mood, and anxiety disorders (5, 6). Active coping in response to stressors is psychosocial factor associated with resilience against stress induced mood and anxiety disorders(7). The neural circuitry underlying active coping is poorly understood but the functioning of these circuits could be key for overcoming anxiety and related disorders (8, 9). Available evidence indicates that active (e.g., escape, fighting) and passive (e.g., freezing, immobility) coping responses to stressors are governed by separable neural circuits (1, 10, 11). The neural circuits, cells, and mechanisms underlying active coping strategies remain unclear (12, 13).

The supramammillary nucleus (SuM) has been suggested to be engaged by threat and found to have efferent connections to stress-sensitive brain regions (14-16). Although anatomic studies indicate SuM is extensively connected to other brain areas, a focus of research on SuM has been on connections to the hippocampus and SuM projections to brain areas remain less understood(15, 17, 18). Recent efforts have shown that SuM contains distinct populations with functionally diverse roles (19-23). In addition to functional diversity, anatomical and molecular-cellular diversity has been found within the SuM(24-26). Divergent populations in SuM have be defined by anatomical, by differential to the dentate gyrus and CA2 regions of the hippocampus, and neurochemically based on neurotransmitter expression (27, 28). Major projections from the SuM, which has yet to be examined, include the preoptic hypothalamus area (POA). Neurons in the POA can regulate a wide range of behaviors and physiological responses including sleep, anxiety, mating, and thermogenesis behaviors, which may be relevant to SuM(29-36).

We identified a unique population of glutamatergic SuM neurons that project to the POA. Using retrograde adeno associated viral (AAV) and combinatorial genetic tools we delineated the extensive arborization of these cells, identifying projections to brain nodes which mediate various features of the stress and threat response including the paraventricular nucleus (PV), periaqueductal gray (PAG), and the habenula (Hb). Here we report that the POA projecting subset of SuM neurons are activated by acute threatening stressors, based on fiber photometry measurements. We found that selective photoactivation of the target SuM population drives aversive and active coping behaviors. Furthermore, activation of these SuM neurons is sufficient to convert passive coping strategies to active behaviors. These findings indicate new circuit mechanisms which governs state transitions between active and passive responses to stress offering opportunities for furthering our neurobiological understanding of stress while helping to identify putative treatments for common psychiatric conditions.

Results

VGLUT2+ SuM neurons send dense projections to the POA

The SuM has efferent projections to many brain regions and contains functionally diverse and anatomically distinct populations(16, 24, 37, 38). These include glutamatergic, GABAergic, and co-expressing GABAergic/Glutamatergic populations (21, 39). To determine whether glutamatergic, VGLUT2 expressing (VGLUT2+), SuM neurons project to the POA we stereotactically injected AAV5-DIO-ChR2eYFP into the SuM and Retro-AAV2-DIO-tdTomato into the POA (**Figure 1A**) of VGLUT2-IRES-Cre mice (n=4). Cells labeled by eYFP were present around the injection site in SuM and eYFP labeled processes in the POA, with dense labeling in the lateral preoptic area (LPO) within the POA (**Figure 1D-E**) were evident. TdTomato expressing soma were present in SuM indicating infection of terminals in the POA by the Retro-AAV (**Figure 1F-G**). Taken together this series of anterograde and retrograde tracing data indicate that VGLUT2+ neurons in SuM project to the POA.

Prior studies have described glutamatergic, GABAergic, and dual (GABA and glutamate) fast neurotransmitter expressing populations within the SuM (23, 39). To examine whether SuM neurons that do not express GLUT2 also project to the POA we used a viral construct encoding for a nuclear restricted fluorophore that switches from expressing mCherry (red) -to- eGFP (green) in a Cre-dependent manner (Retro-AAV2-Nuc-flox(mCherry)-eGFP). This construct expresses mCherry in infected Cre negative cells and eGFP in Cre expressing cells (40). We injected Retro-AAV2-Nuc-flox(mCherry)-eGFP into the POA of VGLUT2-Cre mice (n=4) and examined expression of mCherry and eGFP within the POA and SuM (**Figure 1J**). In the POA we observed

Figure 1

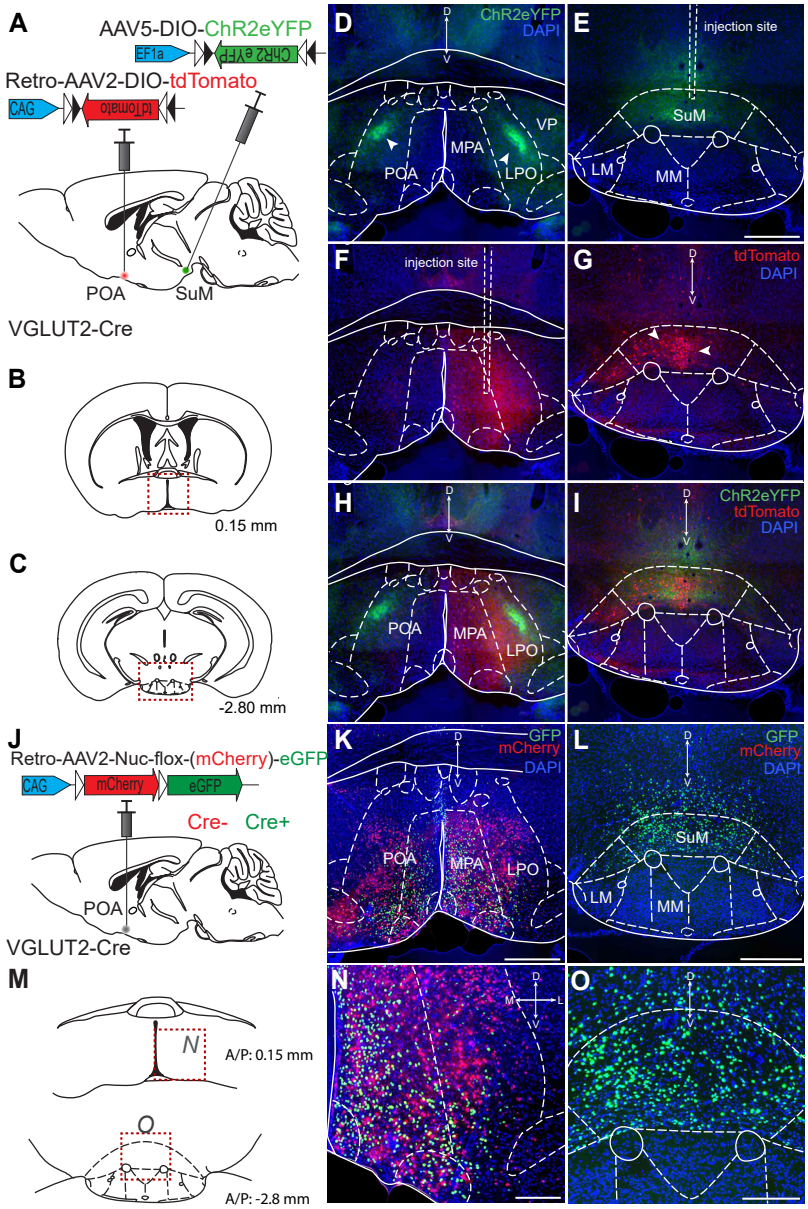

Figure 1. SuM$^{VGLUT2+}$ neurons project to the preoptic area of the hypothalamus. (**A**) Schematic of injections into VGLUT2-Cre mice of Retro-AAV-DIO-tdTomato into the POA and AAV-DIO-ChR2eYFP into the SuM. (**B, C**) The brain regions, POA and SuM, shown in D-I. (**D and E**) Projections of VGLUT2+ SuM neurons and evident in the POA with dense labeling in LPO and the site of viral injection in SuM (500um scale bar). (**F and G**) Show site of injection of in POA and tdTomato labeled cell bodies in SuM. (**H and I**) Overlays of antero- and retrograde labeling from D-G). (**J**) Schematic of injection in POA of fluorophore switching construct in Retro-AAAV in VGLUT2-Cre mice. (**K**) Section containing POA showing eGFP (Cre+) and mCherry (Cre-) labeling near the injection site. (**L**) Section containing SuM showing only eGFP (Cre+) cells. (**M**) The brain regions shown in N and O at high magnification. (**N**) Higher magnification of POA containing section with eGFP (green, Cre+) and mCherry (red, Cre-) seen in the POA near the injection site. (**O**) Higher magnification view of SuM with only Cre positive neurons labeled by eGFP present. (100um scale bar)

cells expressing both mCherry and eGFP (**Figure 1 K and N**) indicating that VGLUT2 negative and VGLUT2 expressing cells were both infected near the injection site**.** In the SuM, however, we only found cells labeled with by eGFP, indicating that all SuM neurons projecting to the POA (SuM::POA) neurons are indeed VGLUT2 expressing. We carried out a parallel experiment in VGAT-Cre mice (n=3) to examine if GABAergic cells in SuM project to the POA. In these mice we observed only mCherry expression in the SuM (**Figure 1 supplement 1**) indicating that VGAT expressing SuM neurons do not send long range projections to the POA. Together, these complimentary anterograde and retrograde tracing methods indicate that SuM neurons projecting to the POA are VGLUT2+ and VGAT- (SuM^{VGLUT2}::POA).

SuM^{VGLUT2}::POA neurons arborize and project broadly throughout the brain

The SuM has extensive efferent projections, and it was recently reported that SuM neurons may arborize (15, 41). To examine the possible arborization of $SuM^{VGLUT2+}$::POA neurons we utilized a combination of Cre (DIO) dependent fluorophore expression and Flp recombinase dependent (fDIO) expression of Cre in mice (VGLUT2-Flp) that express Flp recombinase in VGLUT2 expressing cells. Into the POA we injected Retro-AAV2-DIO-eYFP and into the SuM we injected AAV-fDIO-Cre (**Figure 2A**). We thus expressed Cre in $SuM^{VGLUT2+}$ neurons and, of those, only neurons projecting to the POA (SuM^{VGLUT2}::POA neurons) were labeled with eYFP. Six weeks after injection we collected brain sections and examined them for eYFP labeling. As expected, neurons in SuM were labeled by eYFP (**Figure 2C**). Similar to the results obtained using anterograde tracing in VGLUT2-Cre mice (**Figure 1**), we observed eYFP labeled projections in the POA, particularly in the lateral preoptic area (LPO) (**Figure 2B**). We also identified $SuM^{VGLUT2+}$::POA collaterals to additional brain regions including: the nucleus accumbens (Acb), Septum, later hypothalamus (LH), ventral medial hypothalamus (VMH), paraventricular nucleus (PV), lateral habenula (lHb), the ventral lateral periaqueductal gray (VLPAG), dorsal raphe (DRD), lateral parabrachial nucleus (LPBN), laterodorsal tegmental nucleus (LDTg), and medial vestibular nucleus (MVe) (**Figure 2 D-L**). Complimentary results were obtained in VGLUT-Flp mice 3 with eYFP and 3 using ChR2-eYFP, supporting that our observations were not isolated to a single viral expression type.

To visualize arborization of SuM^{VGLUT2}::POA neurons we injected additional VGLUT2-Flp mice (n=3) with Retro-AAV2-DIO-eYFP into the POA and AAV-fDIO-Cre into the SuM as in **Figure 2A** and then they were actively cleared using SHIELD for optical light sheet imaging (42). The compiled three-dimensional images of a brain hemisphere viewed from the medial to lateral perspective (**Figure 2M**) or viewed from the ventral to dorsal perspective (**Figure 2 supplement**

Figure 1 S1

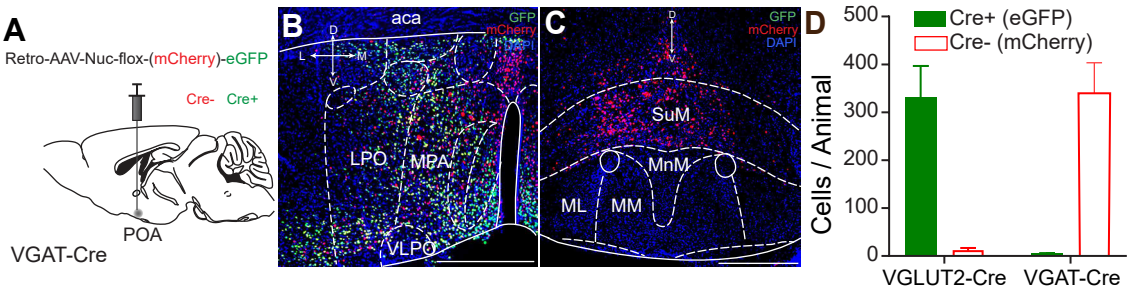

Figure 1 Supplement 1. SuM neurons projecting to the POA are not VGAT+. (**A**) A schematic of the injection of Retro-AAV-Nuc-Flox-(mCherry)-eGFP virus into the bilateral POA in VGAT-Cre mice. (**B**) Cre negative, labeled by mCherry (red) and Cre positive, labeled by eGFP (green), neurons near the injection site in the POA. (**C**) Only Cre negative, mCherry (red) expressing, neurons were seen in the SuM. (500µm scale bar) (**D**) In sections containing SuM from VGLUT2-Cre (n=3) and VGAT-Cre (n=3) injected in POA with Retro-AAV-Nuc-Flox-(mCherry)-eGFP mice cells in SuM labeled by mCherry or eGFP were counted and the mean ± SEM number of cells is plotted.

Figure 2. SuM$^{VGLUT2+}$::POA arborize widely in the brain. (A**)** Schematic of injections of Retro-AAV-DIO-eYFP in to the POA and AAV-fDIO-Cre into the SuM of VGLUT2-Flp mice to label only VGLUT+ SuM neurons that project to the POA. (**B**) Projections of VGLUT2+ SuM neurons labeled with eYFP seen in the POA. (**C**) Cell bodies labeled with eYFP in the SuM. (**D-L**) Arborizing processes from the SuM$^{VGLUT2+}$::POA neurons are seen in multiple brain regions including the(**D**) AcbSh and AcbC; (**E**) lateral septum; (**F**)multiple hypothalamic areas; **G**) LHb and PV; (**H**) the PAG and the DRD; (**I**) VLPAG and LPB; (**J**) DRI and LDTg; (**K**) and DRI, and MVePC. (**M**) Light sheet microscopy image of a cleared mouse brain hemisphere, viewed from medial to lateral, showing eYFP labeled neurons in SuM$^{VGLUT2+}$::POA neurons with cell bodies in SuM and processed in the areas corresponding to septum, hippocampus, Acb, and POA. (500 µm scale bars)

Abbreviations- *MPA* -medial preotic, *VLPO*- ventral lateral preoptic, *LPO*- lateral preotic, *HDB*- nucleus of the horizontal limb of the diagonal band *AcbSh*-Accumbens shell, *AcbC*- Accumbens core, *Shi*- septohippocampal nucleus, *LSI*- lateral septal nucleus, intermediate part, *LSV*- lateral septal nucleus, ventral part, *LV*-lateral ventricle, *MS*- medial septal nucleus, *LHb*-lateral habenula, *MHb*- medial habenula, *PV*- paraventricular thalamus, *DM*-dorsomedial hypothalamic nucleus, *LH* lateral hypothalamic area, *VMH*- ventromedial hypothalamic nucleus, *PAG*- periaqueductal gray, *DMPAG*- dorsomedial periaqueductal gray, *DLPAG*- dorsolateral periaqueductal gray, *LDTg*- laterodorsal tegmental nucleus, *LPAG*- lateral periaqueductal gray, *DRD*- dorsal raphe nucleus, dorsal part, *LPB*- lateral parabrachial nucleus, *MPB*- medial parabrachial, *scp*- superior cerebellar peduncle, *Bar*- Barrington's nucleus, *DTg*- dorsal tegmental nucleus, *DRI*- dorsal raphe, interfascicular part, *LC*- locus coeruleus, MVe medial vestibular nucleus, *4V*- fourth ventricle

Figure 2

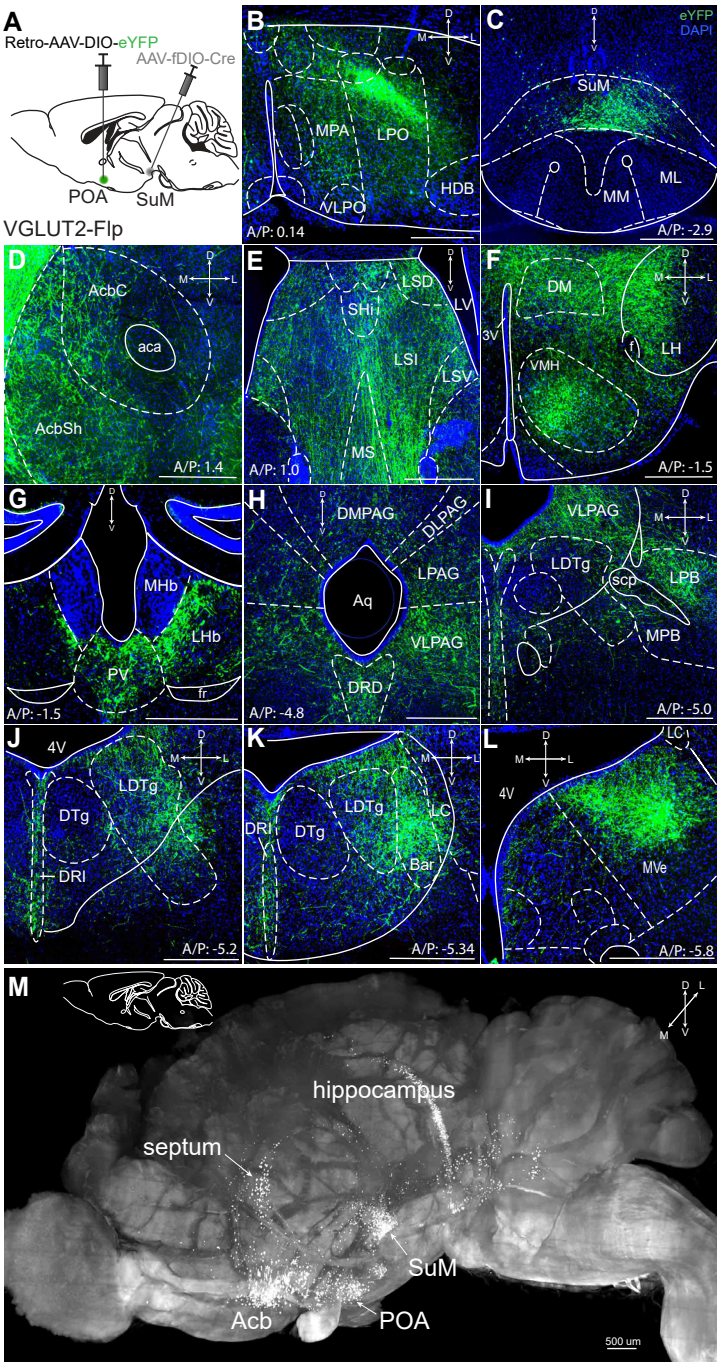

Figure 2 S1

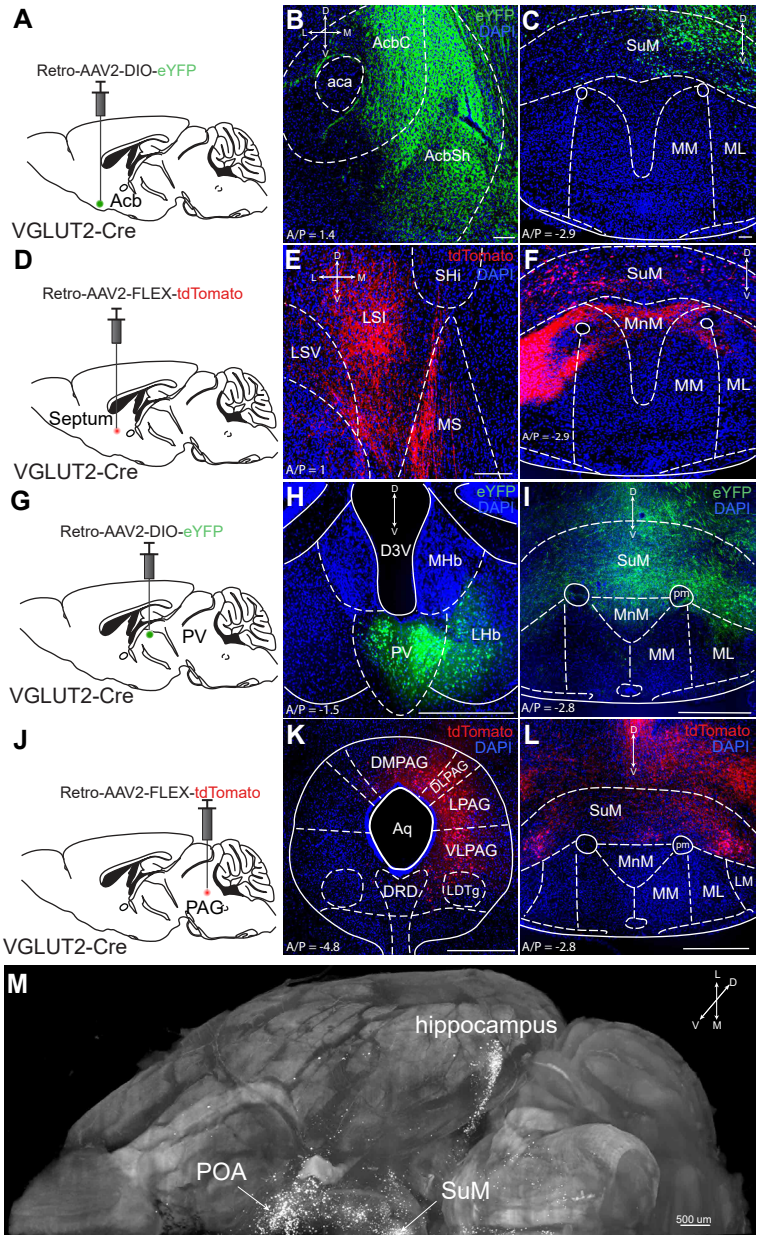

Figure 2 Supplement 1. Retrograde verification of select projection targets of SuM$^{VGLUT2+}$::POA. (**A, D, G, and J**) Schematic showing the injection sites of Retro-AAV's in VGLUT2-Cre mice. (**B-C**) In VGLUT2-Cre mice injection of Retro-AAV-DIO-eYFP unilaterally in the (**B**) accumbens nucleus resulted in labeling of cell bodies in (**C**) SuM. (E-F) Similarly, injection of Retro-AVV-DIO-tdTomato into (**E**) septum resulted in labeling of cell bodies in (**F**) SuM. (**H-I**) injection of Retro-AAV-DIO-eYFP targeting the (**H**) PV and LHb resulted in cell bodies in (**I**) SuM being labeled with eYFP. (**K-L**) Retro-AVV-DIO-tdTomato injected into (**K**) PAG labeled cells in (**L**) SuM. (**M**) The cleared brain hemisphere from a VGLUT2-Flp mouse injected in the POA with injected Retro-AAV-DIO-eYFP show in Figure 2M displayed from a perspective of ventral to dorsal showing cells labeled in SuM and processes extending widely including in the hippocampus and POA. (100 and 500 µm scale bars)

2M) showed projections labeled by eYFP originating from SuM$^{VGLUT2+}$::POA going to POA, the hippocampus, septum, and Acb. Full volume imaging identified projections from SuM$^{VGLUT2+}$::POA neurons to multiple brains areas, establishing broad arborization of the this SuM neuronal population.

In retrograde tracing experiments, we injected Retro-AAV's into brain regions identified by anterograde studies as receiving inputs from SuM$^{VGLUT2+}$::POA neurons. Specifically, Retro-AAV's were injected unilaterally into the Acb, septum, PV, or PAG in VGLUT2-Cre mice. For each area injected with Retro-AAV cell bodies in SuM were labeled by expression of the fluorophore (eYFP or tdTomato) (**Figure 2 Supplement 1**). Each of the 4 areas was injected in three or more mice yielding similar results.

To examine if SuM::POA neuron are anatomically segregated in SuM we injected Retro-AAV2-Cre into the POA and Retro-AAV2-Nuc-flox(mCherry)-eGFP into the SuM (**Figure 2 supplement 2A-B**). In the SuM from brains of wildtype mice (n=3) injected with this combination of viruses we observed both neurons labeled by mCherry (Cre negative) or eGFP (Cre expressing) interspersed in the SuM indicating that the SuM$^{VGLUT2+}$::POA population is not anatomically segregated within the SuM and represents a key subset of SuM neurons.

We performed multiple control experiments to verify that the combinatorial viral approach we used to selectively label SuM$^{VGLUT2+}$::POA neurons had minimal background. In Ai14 reporter mice, which express tdTomato in a Cre recombination dependent manner, we injected Retro-AVV-Flpo into the POA and AAV-fDIO-Cre into the SuM(43). This resulted in labeling of cells in SuM (**Figure 2 supplement 2 G and H**). As a negative control, we injected only AVV-fDIO-Cre into the SuM in Ai14 mice. In these animals we did not observe tdTomato expression (**Figure 2 supplement 2 C-D).** These results demonstrated that the fDIO-Cre construct did not mediate recombination in the absence of Flp recombinase. To confirm that the combination of Retro-AAV2-fDIO-Cres and AAV5-DIO-ChR2eYFP did not lead to labeling of cells with eYFP in the absence of Flp, in wild type mice we injected Retro-AAV2-fDIO-Cre into the POA and AAV-DIOChR2eYFP into SuM. In these mice we did not observe any expression of eYFP (**Figure 2 supplement 2E-F**) confirming dependence on Flp. The results further demonstrate that the specificity of our combinatorial viral strategy we used to establish the arborization and projections of SuM$^{VGLUT2+}$::POA neurons.

SuM$^{VGLUT2+}$::POA neurons represent a subset of SuM$^{VGLUT2+}$ neurons.

Recent studies have highlighted functionally divergent roles of SuM neurons and suggested that differential projections, particularly to regions of the hippocampus and PV, may identify functionally distinct populations (19, 20). To examine if SuM$^{VGLUT2+}$::POA neurons are a

Figure 2 S2

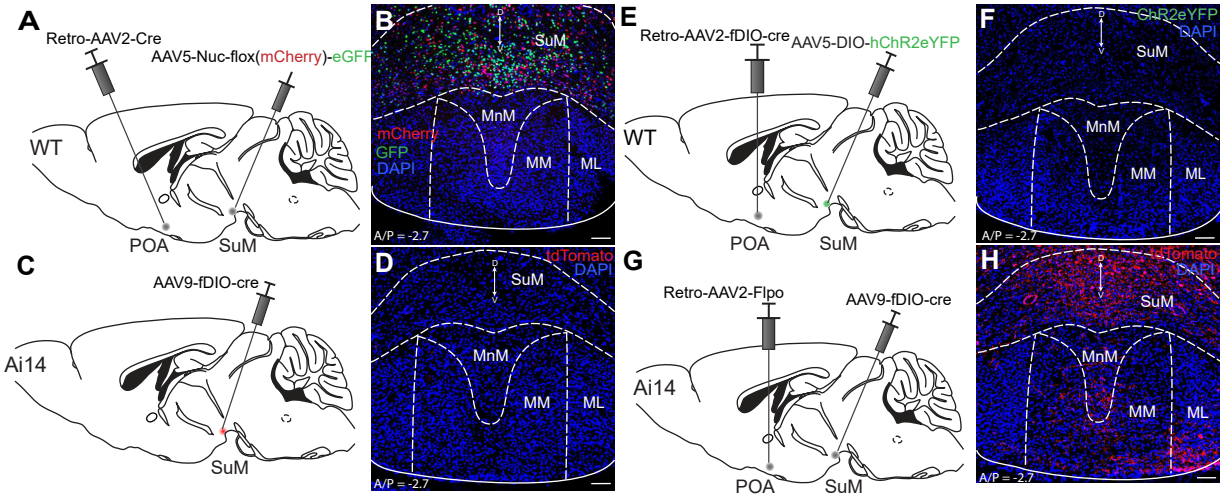

Figure 2 Supplement 2. Subset of SuM neurons labeled by retrograde AAV and combinatorial viral and genetic approach is effective with minimal background. (**A**) Schematic of injection of Retro-AAV-Cre into the POA and AAV-Nuc-flox(mCherry)-eGFP into the SuM of WT mice. (**B**) In SuM eGFP (green) Cre positive and mCherry (red) Cre negative labeled neurons are seen based on expression of Cre mediated by POA injected retrograde AAV constructs. (**C-D**) In Ai14 reporter mice injected with AAV-fDIO-Cre into SuM tdTomato expression indicating recombination is not observed. (**E-F**) In wildtype mice injected in POA with Retro-AAV-fDIO-Cre and in SuM with AAV-DIO-ChR2eYFP expression of ChR2eYFP (green) isd not seen. (**G-H**) In Ai14 mice injected in the POA with Retro-AAV-FlpO and in SuM with AAV-fDIO-Cre cell bodies labeled by tdTomato (red) expression is observed. (100 µm scale bars)

Figure 3

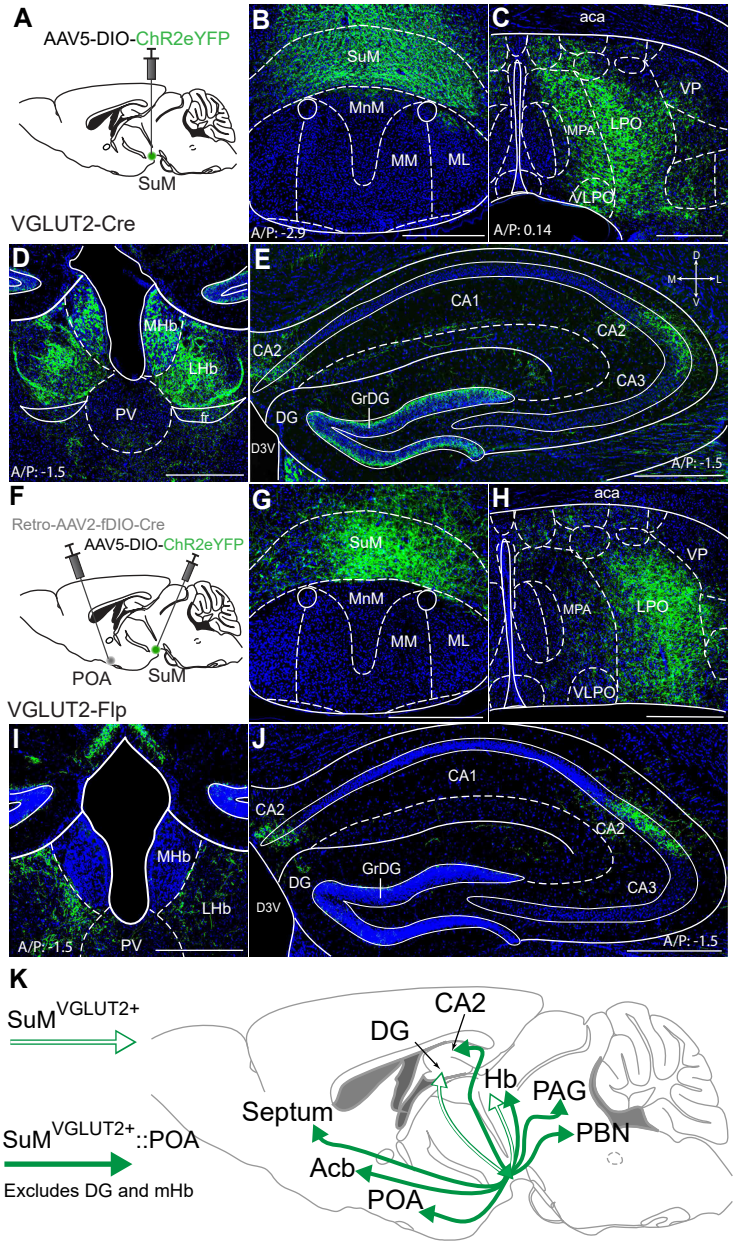

Figure 3. SuM$^{VGLUT2+}$::POA neurons project to a subset of brain regions compared to all SuM$^{VGLUT2+}$ neurons. (**A**) Schematic of injections in VGLUT2-Cre mice of AAV-DIO-ChR2eYFP into SuM. (**B**) eYFP (green) labeled neurons present in SuM and (**C**) processes were observed in the POA. (**D**) Process from SuM VGLUT2+ neurons were also present in MHb, LHb and PV. (**E**) In hippocampus process were observed in DG and CA2. (**F**) Schematic of injections in VGLUT2-Flp mice of Retro-AAV-fDIO-Cre and AAV-DIO-ChR2eYFP into SuM. (**G-H**) Cells in SuM and process in POA were labeled by ChR2eYFP. (**I**) Labeled processes in LHb were evident but none seen in MHb. (**J**) In hippocampus, labeled processes were present in CA2 but not observed in DG. (500 µm scale bars) (**K**) Schematic summary of examined projections showing the projection to DG and MHb present in the total SuM VGLUT2+ population (outlined arrows) but absent in the SuM$^{VGLUT2+}$::POA population (filled arrows).

subset of SuM$^{VGLUT2+}$ neurons we compared the areas with projections from SuM$^{VGLUT2+}$ neurons to those receiving projections from SuM$^{VGLUT2+}$::POA. To label the broader population of VGLUT2+ neurons in SuM we injected AAV5-DIO-ChR2eYFP into the SuM of VGLUT2-Cre mice and after six weeks collected brain sections. In brains from VLUGT2-Cre mice we observed labeled projections from SuM$^{VGLUT2+}$ neurons in the POA, PV, medial habenula (MHb), LHB, the dentate gyrus (DG), and the CA2 field of the hippocampus (**Figure 3 A-E**)**.** Comparing these results to those we obtained used VGLUT2-Flp mice and combinatorial viral constructs to label the SuM^{VGLUT2}::POA population (**Figure 2**), we discovered that projections to the DG and MHb, are present in the SuM$^{VGLUT2+}$ population, but absent in SuM$^{VGLUT2+}$::POA neurons. Projections to the CA2 field and PV were present in both the SuM$^{VGLUT2+}$::POA and the larger SuM$^{VGLUT2+}$ population (**Figure 3D–J**). As schematized (**Figure 3K**) projections from SuM$^{VGLUT2+}$ include projections to DG and mHB which we did not observe in projections from SuM^{VGLUT2}::POA. These findings indicate the SuM$^{VGLUT2+}$::POA population is a subset of the SuM$^{VGLUT2+}$ neuronal population with distinct projection targets and, suggest functionally discrete roles to those previously ascribed to SuM neurons to date.

Acute stress recruits SuM$^{VGLUT2+}$::POA neurons

Prior studies have indicated that SuM neurons can be activated by diverse acute stressors (14, 44, 45). We sought to employ an assay that did not require training, was temporally constrained, well established, and offers the animal both active and passive coping options. The forced swim assay meets these requirements and is increasingly understood as an assay of coping strategy (46, 47). To examine activation of SuM neurons by acute stressors we subjected wildtype mice to 15 minutes of forced swim (n=4) and compared them to control mice that remained in the home cage (n=4). We harvested brains 90 minutes after the forced swim and probed sections containing the SuM with anti-Fos antibodies to examine if Fos expression was induced in SuM neurons after an acute stressor (**Figure 4**). Quantification of cells labeled by anti-Fos antibodies in SuM revealed a significant (p=0.029) increase in cells positive of induction of Fos expression following forced swim (**Figure 4C**). To examine if SuM$^{VGLUT2+}$::POA neurons are activated by acute stress we injected VGLUT2-Cre mice (n=4) bilaterally in the POA with Retro-AAV2-DIO-mCherry and subjected them to forced swim. We probed sections containing SuM with anti-Fos revealing that SuM$^{VGLUT2+}$::POA neurons marked by mCherry expression were positive for induction of Fos expression after forced swim

To further examine if SuM$^{VGLUT2+}$::POA neurons are activated by acute stressors we employed *in vivo* Ca^{2+} imaging using fiber photometry. We injected VGLUT2-Flp mice with AAV9-

Figure 4

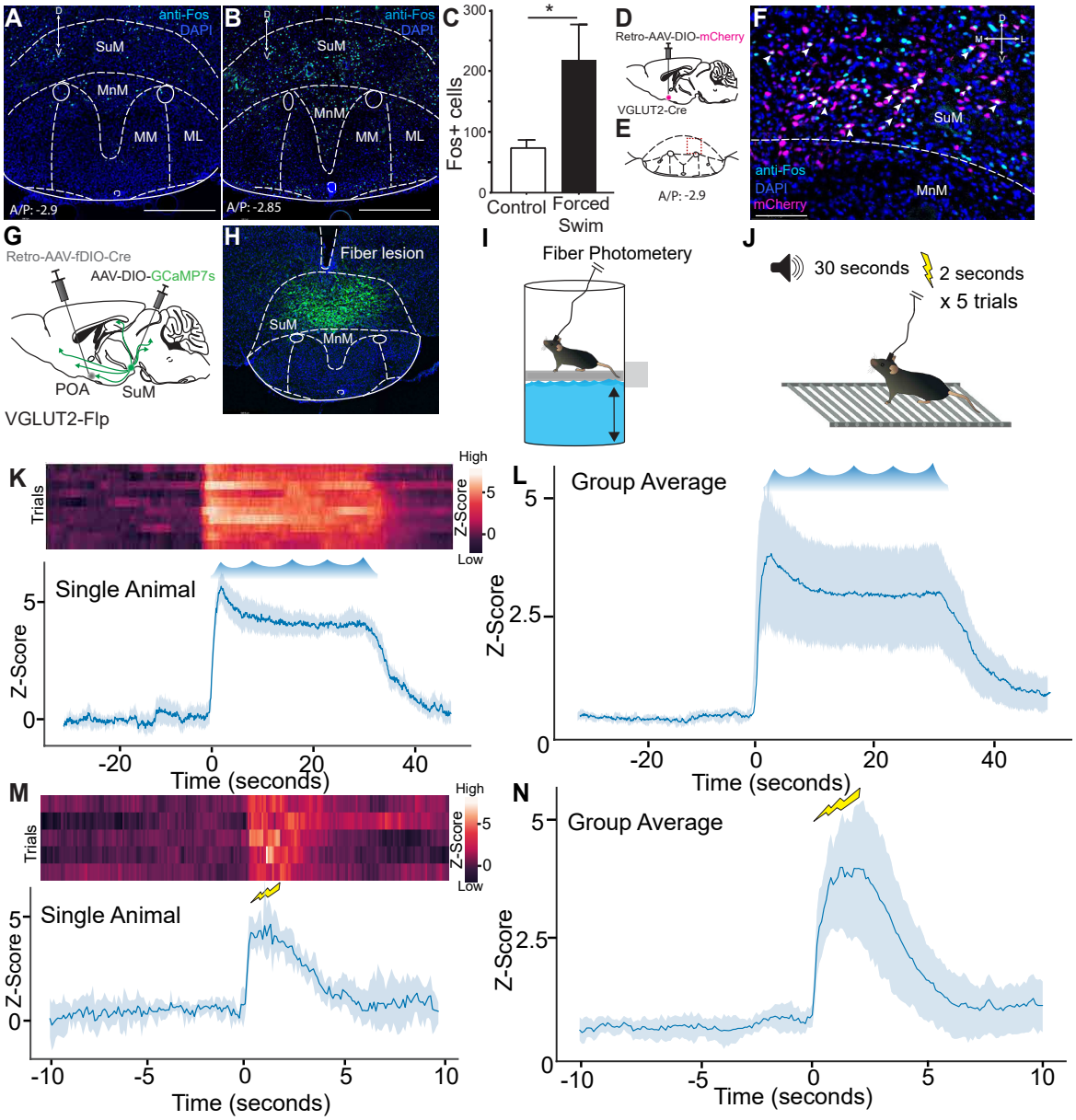

Figure 4. SuM$^{VGLUT2+}$::POA neurons are activated by acute stressors. Sections of brains from mice (**A**) left in the home cage or (**B**) subjected to 15 minutes of forced swimming 90 mins prior to sacrifice were probed with anti-Fos antibodies (cyan) showed (scale bars 500µm) (**C**) a significant (p= 0.029) increase in them mean ±SEM number of anti-Fos labeled neurons in brains from mice subjected to force swim (n=4) compared to control mice (n=4). (**D**) In VLGUT2-Cre mice Retro-AAV-DIO-mCherry was injected in the POA of mice (n=4) subjected to 15 minutes forced swim. (**E**) Region of SuM shown with higher magnification in (**F**) where SuM$^{VGLUT2+}$::POA neurons labeled by mCherry show overlap with cells (arrows) labeled by anti-Fos. (scale bar 100µm) (**G**) Schematic of VGLUT2-Flp mice injected with AAV-DIO-GCaMP7s in SuM and Retro-AAV-fDIO-Cre in the POA with a (**H**) fiber placed over SuM for fiber photometry recordings from SuM$^{VGLUT2+}$::POA neurons. (**I**) Mice were connected for fiber photometry and subjected to 10 30-second trials of forced swimming. (**J**) While fiber photometry recordings were made, SuM$^{VGLUT2+}$::POA neurons mice were subjected to a 2-second foot shock following a 30 second tone for five trials. (**K**) Representative heat map for recordings obtained from a single animal during the repeated forced swim showing increase Ca^{2+} signal during the swim session with the mean ±95% confidence interval of the 10 trials for same animal. (**L**) The mean ±95% confidence interval for Z- score of 10 trials for all 6 animals in the swim assay. (**M**) Representative heat map for recordings obtained from a single animal during the shock trials showing increase Ca^{2+} signal with onset of the shock with the mean ±95% confidence of the 5 trials for same animal. (**N)** The mean ±95% confidence interval Z- score of 10 trials for all 6 animals in the foot shock assay.

DIO-GCaMP7s in the SuM and Retro-AAV2-fDIO-Cre in the POA bilaterally (**Figure 4G**)(48). This yielded expression of GCaMP7s in only SuM$^{VGLUT2+}$::POA neurons (**Figure 4H**). To examine if acute stressors drive activation of SuM neurons, we devised a testing platform that allowed us to initiate and terminate swimming stress without touching the animal (dunk tank) (**Figure 4J**). Animals were habituated to the testing arena but not placed in the water for 3 days prior to testing. On the testing day mice were dunked into the water for a 30-second swim trial every 2 minutes for a total of 10 trials (n=6 mice). We then analyzed the recorded isosbestic and GCaMP signals in the period around each dunk. These analyses revealed rapid robust increase in the GCaMP signal indicating activation of SuM$^{VGLUT2+}$::POA neurons by the swim trials. The mean ±95% CI z-score of GCaMP fluorescence was significantly (p= 0.0078) higher during the dunk compared to baseline. The signal rose rapidly at the onset of swim trial and persisted during the swim trial (**Figure 4L and M**) demonstrating that SuM$^{VGLUT2+}$::POA activity is recruited by acute swim stress.

To determine if other stressors also lead to activation of SuM$^{VGLUT2+}$::POA neurons we used a foot shock paradigm. VGLUT2-Flp mice (n=6) were injected with Retro-AAV2-fDIO-Cre in the POA and AAV-DIO-GCaMP7s in the SuM and then implanted over the SuM with a fiber. Following habituation mice were subjected to five pseudo randomly spaced trials with 30 seconds of tone proceeding a two-second shock. We observed a rapid increased in the GCaMP7s signal following the foot shock (**Figure 4K**). The mean z-score following shock onset was significantly (p= 0.031) higher than baseline (**Figure 4N-P**). Together, these Fos induction and fiber photometry data show that SuM$^{VGLUT2+::}$POA neurons are activated during acute stress.

Photostimulation of SuM$^{VGLUT2+}$::POA neurons evokes active coping behaviors

To understand how activation of SuM$^{VGLUT2+}$::POA neurons may modulate behavior we carried out experiments to assess the types of behavior evoked by photostimulation of SuM$^{VGLUT2+}$::POA neurons. VGLUT2-Cre or wildtype mice were injected with Retro-AAV5-DIO-ChR2eYFP in the POA, and an optic fiber placed midline over SuM (**Figure 5A**). The paradigm we employed was a 15-minute trial divided into three 5-minute periods, pre-stimulation, stimulation at 10 Hz, and post-stimulation. Animals were placed into a clear circular arena with a diameter of 18 cm where the floor of the arena was covered with bedding material. To delineate in detail the changes in behavior evoked by photostimulation we examined the full behavioral patterns exhibited by each animal during the trial period. During the trials we observed behaviors that could be fit into nine categories: grooming, immobile, walking, chewing of bedding, rearing, rapid locomotion (movement was limited by the size of the arena), digging (moving bedding towards the tail), treading (moving bedding forward with front paws), and jumping (**Figure 5B**). A

Figure 5

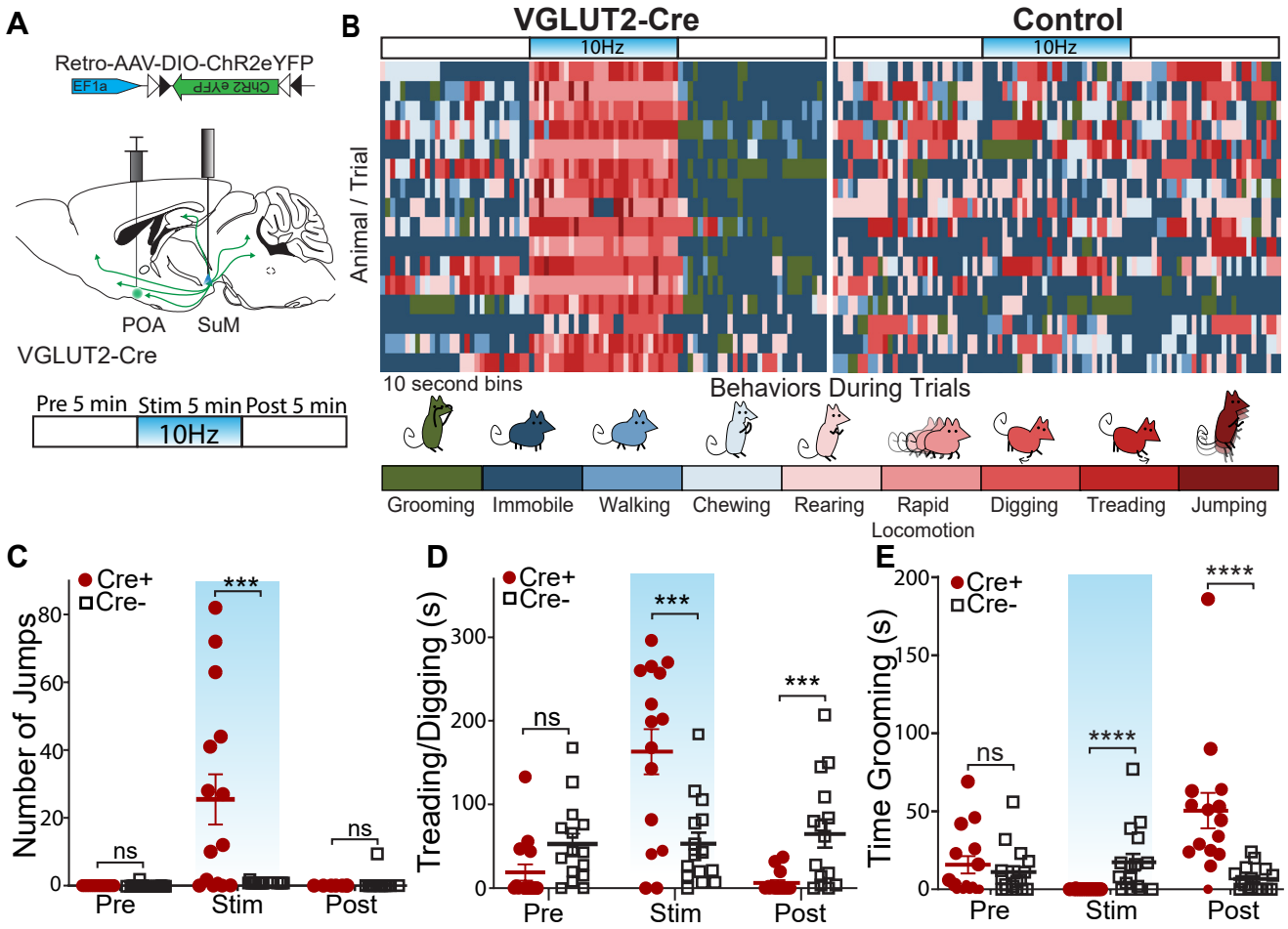

Figure 5. Photostimulation of SuM$^{VGLUT2+}$::POA neurons evokes active coping behaviors. (**A**) Schematic of injections and fiber implant in VGLUT2+ Cre mice and illustration of photostimulation paradigm of 5 min pre, 5 min stimulation, and 5 mins post. Behaviors was evaluated during each epoch. (**B**) During the stimulation period Cre+ (n=15) mice show significantly (p=0.0012) greater jumps than Cre- (n=16) mice and jumping behaviors was not significantly different during pre and post stim periods. (**C**) Behavior was also scored for time spent moving beading (digging or treading). Cre+ mice showed significantly (p=0.004) greater time engaging in digging/treading behaviors during the stimulation period and significantly (p=0.002) less time during the post stimulation period compared to Cre- mice. (**D**) Behavior was also scored for time spent engaging in grooming behaviors and Cre+ mice spent significantly (p<0.001) less time grooming during the stimulation period and significantly (p<0.001) more during the post stimulation period compared to Cre- mice. (**E**) For Cre+ (n=16) and Cre- (n=16) mice the behavior in 10 seconds bins was scored based on the predominate behavior displayed during each 10 period for the 15-minute trial into grooming, stationary, walking, chewing, rearing, rapid locomotion, digging (moving bedding towards the tail), treading (move beading forward), and jumping. The graphic show a by animal scoring of the 15-minute trial color coded for each of the behavior categories. All data plotted as mean ±SEM.

blinded observer scored the behaviors in 10-second intervals for the predominate behavior observed during each interval. Color coded representation of 16 Cre+ and 16 Cre- mice illustrates the broad behavioral changes induced by photostimulation of $SuM^{VGLUT2+}$::POA in Cre+ mice. The behavioral pattern in the pre-stimulation period is similar in between the Cre+ and Cre- mice. During the stimulation period a clear shift to faster locomotion, rearing, treading, digging, and jumping is seen in the Cre+ mice and not the Cre- mice. During the post-stimulation period we observed a new pattern with increased time immobile and grooming compared to the Cre- (control) mice. An example of a Cre+ animal is show in **Supplemental video 1**. The behaviors evoked by photostimulation fit with active coping behaviors. Specifically, escape (jumping, rapid locomotion), defensive burying/treading (digging, pushing beading forward). Quantification of jumping revealed that Cre+ mice (n=16) engaged in significantly (p=0.0012) more jumps during the stimulation period compared to Cre- (n=16) mice (**Figure 5C**). During the pre- and post-stimulation periods there was not a significant difference in the number of jumps. We also noted that the Cre+ mice engaged in bouts of vigorously moving bedding forwards and backwards, as described for defensive burying, during the stimulation period(49).

Defensive burying is characterized by moving bedding forward or backwards often in alternating pattern, is evoked by threatening and noxious stimuli, and is a described active stress coping strategy in rodents(49-52). To minimize risk of artifactual over representation of defensive burying behavior we conservatively quantified together the movement of bedding as treading/digging that may include spontaneous digging (**Figure 5D**). For Cre+ mice compared to Cre- mice there was no significant (p=0.7) difference in the pre-stimulation period. In the stimulation period there was a significant (p=0.004) increase in the time spent treading/digging in Cre+ mice. Surprisingly, in the post-stimulation period time spent engaging in treading/digging was significantly (p=0.0028) decreased in Cre+ mice compared to Cre- mice. The variability in behaviors can be attributed to exclusion of one behavior by the other, with individual mice having variability in the predominant behavior displayed during the photostimulation period but all mice shifted to increased activity coping behaviors.

We also quantified grooming behaviors in each of the three periods (**Figure 5E**). Quantification by a blinded observer revealed no significant difference in time spent grooming during the pre-stimulation period in Cre+ compared to Cre- mice. In the stimulation period the Cre+ mice did not engage in grooming leading to a significant (p<0.0001) decrease in time spent grooming compared to Cre- mice. In the post-stimulation-period Cre+ mice showed a significant (p<0.0001) increase in time spent grooming compared to Cre- mice. A reasonable interpretation

of rise in grooming post stimulation is that photostimulation evoked a stressed like state and cessation of photostimulation led to selfcare grooming as seen following acute stressors (53, 54).

In aggregate, the analysis of behaviors elicited by photostimulation of SuM$^{VGLUT2+}$::POA neurons without conditioned cues or concomitant stressors demonstrates a dramatic shift in behavior to escape oriented (jumping, rapid locomotion) and threat response behavior, including rearing and defensive burying, during the photostimulation period. In contrast to freezing, the behaviors elicited by activation of SuM$^{VGLUT2+}$::POA neurons indicate that they alter active coping strategies.

Photostimulation of SuM$^{VGLUT2+}$::POA **neurons promotes real time avoidance behavior**

Next we injected VGLUT2-Cre or WT mice in the POA with Retro-AAV5-DIO-ChR2eYFP and implanted a single midline optic fiber over SuM to determine if we could promote canonical real time avoidance behavior within this circuit (**Figure 6A**)(55). We carried out real-time place aversion testing (RTPA) by pairing one side of the chamber with blue light stimulation. Each animal was tested at multiple frequencies (**Figure 6B**). Increasing the stimulation frequency produced a progressive increase in the level of aversion, which was statistically significant ($p<0.0001$) at 1, 5, 10 and 20 Hz in Cre+ (n=19) mice compared to Cre- (n=21) control (**Figure 6B and C**). Interestingly, the number of entries to the stim per one minute bin over the course of the experiment was not significantly different between Cre+ and Cre- mice ($p=0.87$ mixed-effects model) (**Figure 6D**), but the mean time spent on the stimulation side of the area was lower ($p<0.0001$ mixed-effects model) in the Cre+ (n=14) that Cre- (n=13) mice (**Figure 6E**). This indicates that Cre+ mice displayed equivalent exploratory behavior as compared to Cre- mice, but quickly, and actively leave the simulation side after each photostimulation triggered event. Surprisingly, these data also indicate that the aversion did not generate aversive pairing during the trial, as seen for photostimulation of other brain areas (56). Examples of Cre+ mice with stimulation at 1, 5, and 10Hz as well as Cre- mice is in **Supplemental Video 2**. To examine the relative aversiveness of SuM$^{VGLUT2+}$::POA photostimulation we carried out RTPA experiments using a modified arena with a dark side and a bright side (**Figure 6F inset**). We paired photostimulation with the dark, preferred side of the arena. As expected, Cre- mice show a preference for the dark side of the arena. Photostimulation of the SuM$^{VGLUT2+}$::POA neurons yielded significant (**$p=0.002$, ***$p=0.0004$, ****$p<0.0001$) aversion of Cre+ (n=13) compared to wildtype (n=12) at tested frequencies (10 and 20Hz) and was sufficient in promoting mice to spend nearly the entire duration of the trial in the typically aversive, brightly light side of the arena during photostimulation (**Figure 6F**). These indicate that photostimulation of SuM$^{VGLUT2+}$::POA is

Figure 6

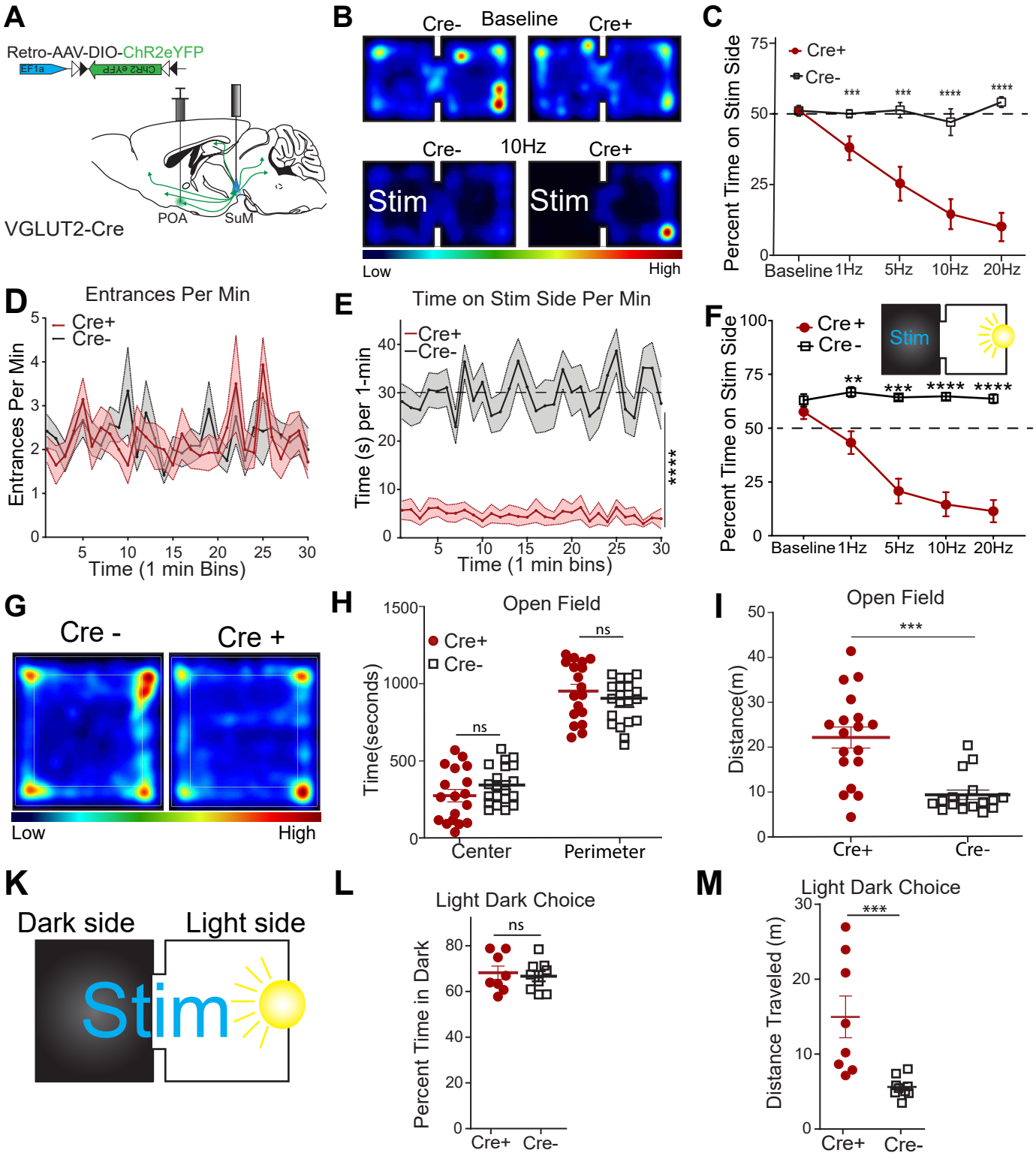
A
Retro-AAV-DIO-ChR2eYFP
EF1a
ChR2 eYFP
POA
SuM
VGLUT2-Cre
B
Cre-
Baseline
Cre+
Cre-
10Hz
Cre+
Stim
Stim
Low
High
C
Cre+
Cre-
Percent Time on Stim Side
Baseline
1Hz
5Hz
10Hz
20Hz
D
Entrances Per Min
Cre+
Cre-
Entrances Per Min
Time (1 min Bins)
E
Time on Stim Side Per Min
Cre+
Cre-
Time (s) per 1-min
Time (1 min bins)
F
Cre+
Cre-
Stim
Percent Time on Stim Side
Baseline
1Hz
5Hz
10Hz
20Hz
G
Cre -
Cre +
Low
High
H
Open Field
Cre+
Cre-
ns
ns
Time(seconds)
Center
Perimeter
I
Open Field
Distance(m)
Cre+
Cre-
K
Dark side
Light side
Stim
L
Light Dark Choice
ns
Percent Time in Dark
Cre+
Cre-
M
Light Dark Choice
Distance Traveled (m)
Cre+
Cre-

Figure 6. Activation of SuM$^{VGLUT2+}$::POA neurons drives aversion but does not promote anxiety-like behavior (**A**) Schematic of injection of Retro-AAV-ChR2eYFP into the POA and placement of a midline optic fiber over SuM. (**B**) Real time place avoidance arena with photo stimulation provided on one side of arena as representative heatmaps for Cre+ and Cre- mice at baseline (no stim) and 10Hz photostimulation. (**C**) Quantification of time spent of stimulation side in ChR2eYFP expressing (Cre+ mice n =19) and control (Cre- mice n=21) mice showing frequency dependent avoidance of the stimulation side of the area on average spending significantly (***p<0.001, ****p<0.0001). (**D**) Mean entrances to the stimulation side of the area quantified in 1-minute bins during 10 Hz stimulation trials were not significantly (p=0.87) different between Cre+ (n=14) and Cre- (n=13) mice. (**E**) Mean time spent on the stimulation side for Cre- and Cre + in 1-minute bins during 10 Hz stimulation trials was significantly (p<0.0001) lower in Cre+ mice. (**F**) Diagram (inset) of light/dark arena with photo stimulation provided on the dark side of the arena quantification of time spent on dark (stimulation) side demonstrating that Cre- (n=12) animals show a preference for the dark side of arena that is overcome by photostimulation with Cre+ (n=13) mice spending significantly (** p=0.002, ***p<0.001, ****p<0.0001) less time on the stimulation side in frequency dependent manner. (**G**) Representative heatmap of Cre- and Cre+ during 10Hz photostimulation in open field test. (**H**) In open field test time spent in center and perimeter were not significantly different (p=0.19) between Cre+ (n=18) and Cre- (n=17) during 10Hz photostimulation. (**I**)Total distance traveled during open field testing was significantly (p<0.001) increased in Cre+ compared to Cre-. (**K**) Schematic of real time light/dark choice testing with stimulation provided at 10Hz throughout the arena. (**L**) Both Cre+ (n=8) and Cre- (n=9) mice showed a preference for the dark portion of the arena but were not significantly (p=0.9) different. (**F**) The total distance traveled by Cre+ mice were significantly (p=0.003) greater than Cre- mice. All data plotted as mean ±SEM.

Figure 6 S1

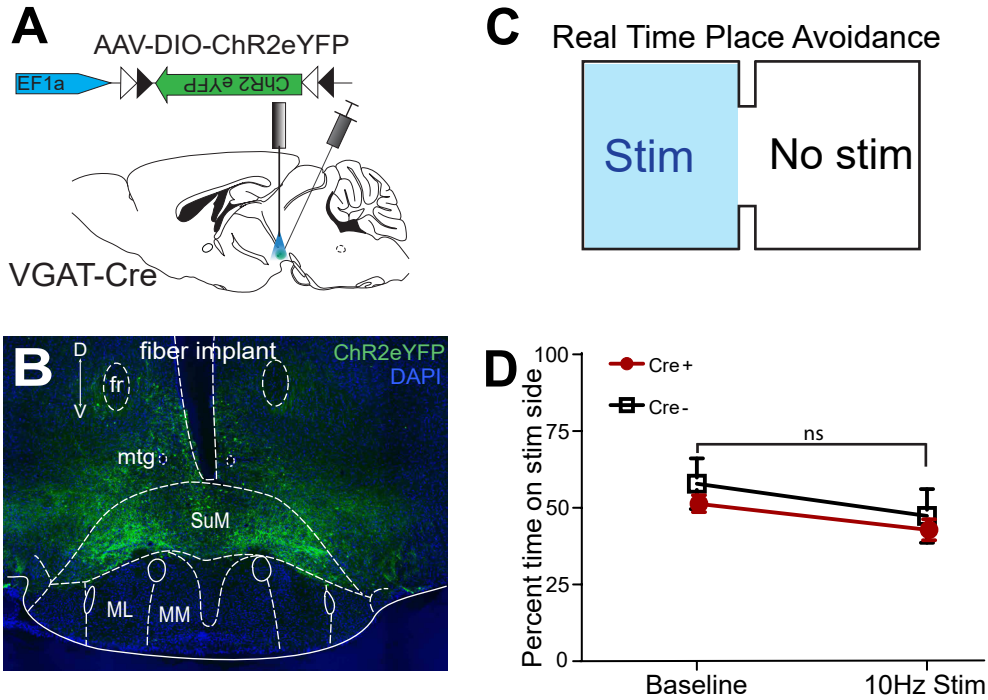

Figure 6 Supplement 1. GABAergic neurons in SuM do not drive place preference. (**A**) Schematic of viral injection into VGAT-Cre mice to express ChR2eYFP in SuM. (**B**) VGAT+ neurons labeled and outline of track from implanted fiber. (**C**) Realtime arena showing the pair of photostimulation on one side of the arena. (**D**) Photostimulation at 10Hz did not drive a significant place preference. (Cre+ n=7 and Cre- n=4). All data plotted as mean ±SEM.

sufficient to robustly promote active avoidance behavior, even in the presence of an already mildly aversive stimulus (bright light).

Reports have described neurons in supramammillary that project to the dentate gyrus of the hippocampus and release both GABA and glutamate. Our anatomic studies (**Figure 3**) indicated that $SuM^{VGLUT2+}$::POA neurons do not project to the dentate gyrus and are not GABAergic based on VGAT expression (**Figure 1S1**). To examine if GABAergic neurons in SuM mediate real-time place aversion or preference, we injected VGAT-Cre (n=7) or Cre- (n=4) mice in SuM with AAV5-DIO-ChR2eYFP (**Figure 6 supplement 1 A-C**) and carried out real-time place aversion testing. With photostimulation set to 10 Hz no significant aversion or preference was evident compared to baseline or Cre- mice (n=4) (**Figure 2 supplement 1 D**), further demonstrating specificity of the functional role of $SuM^{VGLUT2+}$::POA neurons and suggesting that SuM^{VGAT} neurons appear under these conditions to not regulate active coping behavior.

Photoactivation of $SuM^{VGLUT2+}$::POA neurons does not cause the expression of anxiogenic-like behavior.

Acute stressors often induce anxiety-like, risk aversion behavioral states (57-59). To determine whether $SuM^{VGLUT2+}$::POA may also contribute to anxiety behaviors we used two established tests for anxiety-like behavior, the open field and light-dark exploration, in Cre+ and Cre- controls (60-63). Mice were injected in the POA. For open field testing, mice were placed in an open field arena and photostimulation was applied to SuM at 10Hz during the entire trial. We analyzed the position of the animals and quantified the time spent in the perimeter (outer 50%) vs. the center (inner 50%) of the arena. Cre+ (n=18) and WT (n=17) mice were not significantly (p=0.17, and 0.19) different in the time spent in either the center or perimeter areas (**Figure 6H**). We also analyzed the distance traveled and found a significant ($p<0.001$) increase in total distance traveled in Cre+ mice compared to Cre- mice (**Figure 6I**). In the light-dark exploration test we examined if 10 Hz photostimulation of $SuM^{VGLUT2+}$::POA neurons altered the preference for the dark side of a light-dark arena (**Figure 6L**). VGLUT2+ mice (n=8) did not show a significant (p=0.9) increased preference for the darkened side of the arena compared to Cre- (n=9) but did show a significant (p=0.003) increase in total distance moved (**Figure 6M**). The findings obtained in open field and light-dark exploration testing do not support a role for $SuM^{VGLUT2+}$::POA neurons in driving anxiety-like behaviors, suggesting a discrete role for the $SuM^{VGLUT2+}$::POA pathway in activate avoidance behaviors which are distinct from those represented in traditional anxiogenic assays.

Figure 7

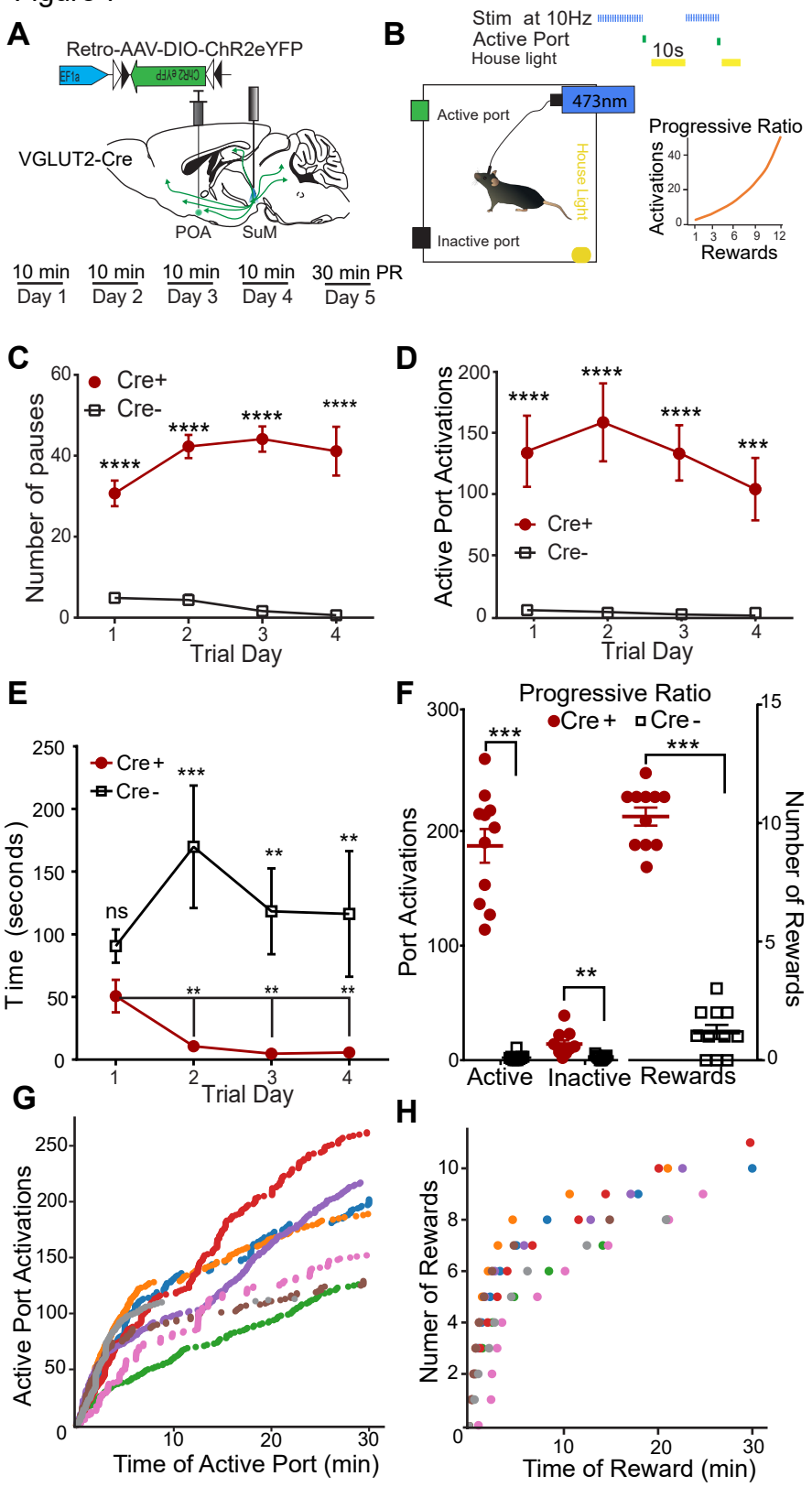
A
Retro-AAV-DIO-ChR2eYFP
EF1a
ChR2 eYFP
VGLUT2-Cre
POA
SuM
10 min Day 1
10 min Day 2
10 min Day 3
10 min Day 4
30 min PR Day 5
B
Stim at 10Hz
Active Port
House light
10s
473nm
Active port
House Light
Inactive port
Progressive Ratio
Activations
Rewards
C
Cre+
Cre-
Number of pauses
Trial Day
D
Active Port Activations
Trial Day
E
Time (seconds)
ns
Trial Day
F
Progressive Ratio
Cre+
Cre-
Port Activations
Number of Rewards
Active
Inactive
Rewards
G
Active Port Activations
Time of Active Port (min)
H
Numer of Rewards
Time of Reward (min)

Figure 7. Photostimulation of SuM$^{VGLUT2+}$::POA neurons is sufficient to drive goal directed behavior in a negative reinforcer operant task. (**A**) Schematic of injection and implant in VGLUT2+ Cre mice and paradigm of testing in 10-minute trials with 4 days before a progressive ratio (PR) trial on day 5. (**B**) Illustration of the testing paradigm and set up. 10Hz photo stimulation was applied during the trials. Activation of the active port trigger the house light and paused stimulation for 10 seconds. Also show is the progressive ratio used with number of required port activations per reward on vertical axis and reward number on the horizontal. (**C**) Cre+ mice (n=11) activated the active port triggering significantly (****$p<0.0001$) more pauses in stimulation than Cre- mice (n=11) mice on all 4 days of testing. (**D**) Cre+ mice activated the port significantly (****$p<0.0001$, ***$p<0.001$) than the Cre- mice on all 4 trials. Cre+ activated the active port significantly ($p<0.001$) on during the fourth trial than the first. (**E**) The time to first activation of the active port was not significantly($p=0.32$) different during the first trial but Cre+ became significantly (**$p<0.01$, ***$p<0.001$) faster than Cre- to activate the active port after onset photostimulation and were faster during the second, third and fourth trial compared to the first trial. (**F**) On the fifth day after four 10-minute trials mice were test for 30 minutes using a progressive ratio test requiring port active port activations to trigger a pause in the photostimulation. Cre+ performed significantly ($p<0.0001$) more active port activations that Cre- mice and activated the inactive port significantly more ($p<0.005$) times. Cre+ mice also triggered significantly ($p<0.001$) more pauses in photostimulation that Cre- mice. (**G**) Individual data for a representative cohort of Cre+ mice showing cumulative active port activations by Cre+ mice (n=7) as function of time during the progressive ratio test are shown illustrated on-going engagement of the active port throughout the 30-minute trial. (**H**) The cumulative pauses in photostimulation (rewards) earned as a function of time during the progressive ratio trial are show for individual Cre+ mice. Mice earn between 7 and 11 pause reward during the trial.

SuM$^{VGLUT2+}$::POA neurons drive operant controlled active avoidance behavior

Threat responses can taxonomically be divided into two broad categories, innate (fixed or Pavlovian) and instrumental (action-outcome and habits) (1). Additionally stress responses can be divided into active vs passive actions. Accumulating evidence indicates that different behaviors in these separable categories are mediated by distinct neural circuits (1, 64). For example, studies on areas involved in responding to specific threatening stimuli (looming threat) drive innate fix responses when activated (8). To determine how SuM$^{VGLUT2+}$::POA neurons fit into this behavioral framework, specifically whether they can evoke innate verses goal-directed behaviors, we developed an operant negative reinforcement paradigm. We hypothesized that if stimulation of SuM$^{VGLUT2+}$::POA evokes innate defensive behavior then performance of an operant task (an action-outcome behavior), should not occur because innate defensive behaviors (ex. escape) would disrupt successful completion of the operant task (nose port activation). Our real-time place aversion demonstrated that photostimulation of SuM$^{VGLUT2+}$::POA neurons is highly aversive and thus could potentially be used as a negative reinforcer. Thus, we devised the following paradigm. In an enclosed area with two nose poke ports (one active and one inactive) that could be activated mice received photostimulation at 10 Hz during a 10-minute trial. Activation of the active port by a nose poke triggered a 10-second pause in photostimulation and turned on a house light for 10 seconds (**Figure 7A and B**). Following this 10 second pause the port was active again and port activation occurring during a pause were counted but did not altered stimulation. To selectively photostimulate SuM$^{VGLUT2+}$::POA neurons, VGLUT2-Cre or Cre- mice were injected with Retro-AAV5-DIO-ChR2eYFP into the POA bilaterally with placement of a midline fiber over SuM (**Figure 7A**). We tested animals for 5 consecutive days. The first four days were 10-minute trials with each activation of the active port during photostimulation triggered a 10-second pause. On the fifth day we employed a 30-minute test using a progressive ratio that required exponentially increasing number of active port activations to trigger a pause in the photostimulation **(Figure 7B**). No training was performed prior to the first test day. Analyses of port activations during the 10-minute trials revealed that Cre+ mice (n =11) paused the photostimulation (reward) significantly ($p<0.0001$) more on all four days of testing compared to Cre- (n=11) mice (**Figure 7C**). The number of 10-second pauses approached the maximum of 60 possible in a 10-minute period. Cre+ mice engaged the active port significantly (****$p<0.0001$, ***$p<0.001$) more than Cre- mice (**Figure 7D**). Interestingly, despite achieving more pauses on average on the fourth day Cre+ engaged the active port significantly ($p=0.009$ paired t-test) fewer times than the first day, suggesting that mice learned greater efficiency at performing the task with increased trials number. The time to the first engagement of the active port was not significantly ($p=0.32$) different

for Cre+ compared to Cre- mice during the first test trial (**Figure 7E**) indicating no difference in baseline performance of the task. During the three subsequent tests Cre+ mice were significantly ($p<0.01$) faster to engage the active port after the start of the trial compared to Cre- mice. Cre+ mice also were significantly ($p<0.01$ paired t-test) faster in trials two through four at engaging the active port compared to their performance on the first trial. During the 30-minute trials using a progressive ratio, Cre+ mice activated the active port significantly ($p<0.001$) more times than Cre- mice (**Figure 7F**). Cre+ mice generated significantly more rewards (pauses in stimulation) than Cre- mice. Individual cumulative activity shows throughout the 30-mintute progressive ratio trials Cre+ mice continue to engage the active port despite the increasing work required to generate each pause in photostimulation (**Figure 7G**) indicating that activation of $SuM^{VGLUT2+}$::POA neurons remains highly salient and motivating. Examining the time point each reward was achieved for individual animals reflects the increasing time required to complete the number of port engagements needed to earn each pause in photostimulation (**Figure 7H**). For the animal with the lowest number of rewards earned (green dots) the next pause required 20 activations of the active port and for the highest (red dots) the next pause required 50 activations of the active port. The trial was limited to 30-minutes due to concern for the welfare of the animals due to the risk they would engage in escape behaviors while in the operant chambers with tethered headcaps if sessions were extended too long. The results from the operant task experiments confirmed the aversiveness of $SuM^{VGLUT2+}$::POA photostimulation. The results also demonstrate that activation of $SuM^{VGLUT2+}$::POA neurons can drive action-outcome instrumental behaviors as an active coping behavior. The progressive ratio testing demonstrated that the activation of $SuM^{VGLUT2+}$::POA neurons remains salient and motivating even when the effort (port activations) required to terminated photostimulation increases and periods of photostimulation between pauses lengthens.

$SuM^{VGLUT2+}$::POA neurons promote active coping

We found that $SuM^{VGLUT2+}$::POA neurons are activated by acute stressors (**Figure 4**) and that photostimulation elicited behaviors typical of active response to threatening or noxious stressors (**Figure 7**) in the absence of environmental stressors. The forced swim test is a stress-based assay that allows mice to select between active (swimming, climbing) and passive (immobile floating) coping strategies with progressive increase in the time spent in the passive state(47). To determine if $SuM^{VGLUT2+}$::POA neurons can regulate the behavioral response to a stressor we used a two-day forced swim stress assay(47, 65). Using VGLUT2-Cre (Cre+) or wildtype (Cre-) mice injected in the POA bilaterally with Retro-AVV-DIO-ChR2eYFP we subject mice to 15 minutes of forced swim and then on the subsequent day we repeated the forced swim

Figure 8

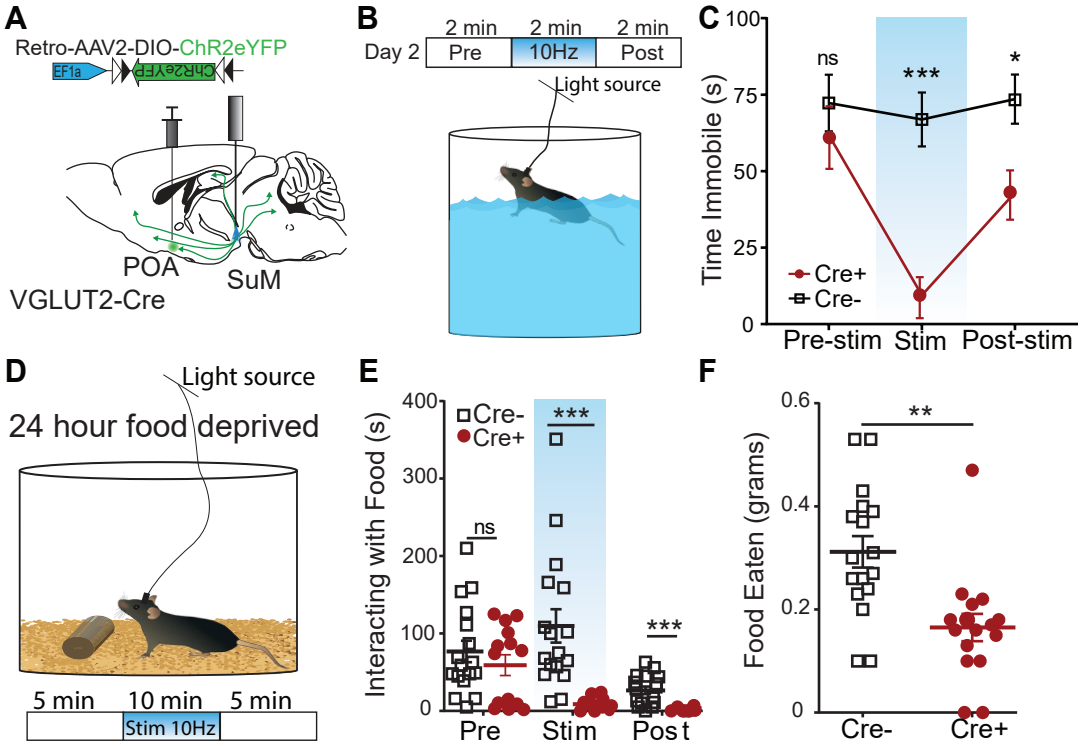

Figure 8. Photostimulation of VGLUT+ SuM→POA neurons increases active coping in forced swim test and redirects feeding behavior in fasted mice. (**A**) Schematic of injection and implant in VGLUT2+ Cre mice. (**B**) Illustration of testing paradigm on second of forced swim test following 15-minute swim on first day. 6-minute trial with forced swim 2 minutes of stimulation applied after a 2-minute pre stimulation period. (**C**) The average time spent immobile during the pre-stimulation period was not significantly (p=0.48) different.10 Hz photostimulation caused Cre+ mice to engage in vigorous swimming and the time spent immobile was significantly (p<0.001) different from Cre- mice. In the post-stimulation period, the time spent immobile remained significantly (0.016) lower in Cre+ mice compared to Cre-. (**D**) Mice were fasted for 24 hours prior to testing and the schematize paradigm was used. The fasted animal was given access to a standard chow pellet for a 20-minute trial divided in to a 5-minute pre- and post-stimulation periods with 10-minute period of stimulation. (**E**) The time spent interacting with the food was quantified for each period. Cre+ (n=16) and Cre- (n=17) mice both rapidly engaged with the food pellet and the average time spent interacting was not significantly (p=0.37) different. During the stimulation period and the post stimulation period the average time interacting with the food was significantly (p=0.0002, p=0.0001) lower in Cre+ mice compared to Cre- mice. (**F**) The food eaten during the total trial was calculated based on pellet weights and on average Cre+ mice ate significantly (p=0.001) less food during the trial than Cre- mice.

for six minutes divided into three periods of two minutes each, pre-stimulation, stimulation at 10Hz, and post-stimulation (**Figure 8A and B**). Trials on the second day were recorded and scored by a blinded observer for time spent immobile by each animal. Example of Cre+ mouse with stimulation 10Hz is in **Supplemental Video 3**. Cre+ (n=9) and Cre- (n=11) mice on average did not spend significantly (p=0.45) different amount of time immobile during the 2-minute pre-stimulation period. During the stimulation period Cre+ mice began swimming and attempting to climb the perimeter of the circular swim arena, resulting in a reduction in immobility (**Figure 8C**). During the stimulation period, the Cre+ mice spent significantly (p<0.0001) less time immobile than Cre- mice. Interestingly, in the post stimulation phase the difference in time spent immobile between Cre+ can Cre- mice diminished but remained significantly (p=0.016) different. These results indicate that in the context of an ongoing stressor activation of $SuM^{VGLUT2+}$::POA neurons is sufficient to trigger a change in coping strategy from a largely passive (floating) to and active (swimming, climbing). The persistent effect of the acute activation into the poststimulation phase suggest that activation of $SuM^{VGLUT2+}$::POA neurons may shift how the stressor is process or approached.

Photostimulation of $SuM^{VGLUT2+}$::POA neurons redirect motivated feeding behavior

From an evolutionary context choosing to feed while also and responding to threats are conflicting actions and $SuM^{VGLUT2+}$::POA neurons may play a role in switching between behavioral paradigms (e.g., feeding vs escape). To examine if activation of $SuM^{VGLUT2+}$::POA neurons redirects behavior in the context of a conflicting motivated behavior we determined the impact of photostimulation on feeding behavior in food deprived mice. Using VGLUT2-Cre or wildtype mice injected with Retro-AAV5-DIO-ChR2eYFP into the POA and implanted with a fiber midline over SuM we examined how feeding behaviors in mice deprived of food for 24 hours were altered by 10 Hz activation of $SuM^{VGLUT2+}$::POA neurons (**Figure 8A and D**). Mice were habituated to a small behavioral arena prior to testing and subjected to food deprivation for 24 hours prior to testing. Mice were then reintroduced to the arena and a chow pellet was added. Mice were allowed access to the pellet for 20 minutes. Each trial was divided into three periods, a 5-minute pre-simulation period, 10-minute stimulation period, and a 5-minute post-stimulation period. Trials were recorded and scored for time spent interacting with the food pellet. The time Cre+ (n=17) and Cre- (n=16) mice spent interacting with the food was not significantly (p=0.37) different in the pre stimulation period. During the stimulation period Cre+ mice spent significantly (p=0.0002) less time interacting with the food as compared to Cre- mice. Surprisingly, the decrease in time spent interacting with the chow pellet continued into the post-stimulation phase with Cre+ mice interacting with the food significantly (p<0.0001) less than Cre- mice (**Figure 8E**). The total decrease in time spent

interacting with food was reflected by the decrease in the amount of food consumed calculated by the change in the weight of the chow pellet during the trial. Cre+ mice consumed significantly (p=0.001) less food during the 20-minute trial than Cre-mice. These results indicate that $SuM^{VGLUT2+}$::POA neurons can redirect behavior away from motivated feeding, in a similar manner to the presentation of a threat. Whether $SuM^{VGLUT2+}$::POA directly encode feeding is not clear. However, studies have suggested that SuM neurons may instead play a role in modulating feeding behaviors (66, 67). Interestingly, three separate assays, unprovoked behaviors (**Figure 7**), forced swim (**Figure 8C**), and food deprivation (**Figurer 8E**) reveal that $SuM^{VGLUT2+}$::POA neuron activation for a brief time leads to altered behavior after photo stimulation ends including increased grooming, greater escape activity, and suppression of feeding respectively. Further investigation of how the distributed $SuM^{VGLUT2+}$::POA neuronal efferents function will be required to understand this neural population influences chronic stress and related behaviors.

Discussion

In order to maximize survival an animal must actively select between active and passive coping strategies to aversive and threatening experiences. Passive coping strategies have been associated with unescapable stress, anhedonia, and depression(7, 68-70). The presented results define a novel population of neurons in SuM ($SuM^{VGLUT2+}$::POA), delineate the broad arborization of these neurons to diverse brain areas, and delineate the functional roles in driving coping behaviors to acute threatening stressors. These findings build on recent reports demonstrating functional diversity in the SuM, expand the known roles of SuM in regulating behavior, and open new avenues for investigation into neural circuits regulating stress coping behaviors by linking SuM neurons to driving negative affective states, threatening stressors, and active coping behaviors.

Here we identified a population of VGLUT2+, VGAT- (**Figure 1 and Figure 1 S1**) SuM neurons that project to the POA and that the $SuM^{VGLUT2+}$::POA neurons arborize widely projecting to many brain areas (**Figure 2**). We found that the projections of $SuM^{VGLUT2+}$::POA neurons have a distinct subset of the broader $SuM^{VGLUT2+}$ neuron projections. Notably, mHb and DG projections were present in the $SuM^{VGLUT2+}$ population but absent in the $SuM^{VGLUT2+}$::POA projections (**Figure 3K**), consistent with a separation of DG and CA2 projecting SuM neurons previously reported (71). The projections to PV, Hb, and PAG are of particular interest because these areas have been implicated in regulating stress coping behaviors(72-75). Recently, dopamine receptor 2 expressing neurons in the PV have been implicated in promoting active coping behaviors and may be a potential target of $SuM^{VGLUT2+}$::POA neurons (10, 11). The habenula has also been

implicated in regulating active vs passive coping behaviors making the selective projections of SuM$^{VGLUT2+}$::POA neurons to the lHb of similar interest (72, 76, 77). In addition, the PAG, which contains processes from SuM$^{VGLUT2+}$::POA neurons, has been implicated in regulating defensive behaviors and coping strategies (73, 74, 78). Thus, SuM$^{VGLUT2+}$::POA neurons are positioned to be critical for modulating behavior by providing concurrent excitatory inputs to multiple region which regulate stress coping.

Using fiber photometry, induction of Fos, and optogenetics we report here that SuM$^{VGLUT2+}$::POA neurons are activated by threatening stressors (forced swim and foot shock) (**Figure 4**), drive a negative affective state (**Figure 5**), to ultimately promote active coping behavior (**Figures 7 and 9**). Surprisingly, we found that photostimulation of SuM$^{VGLUT2+}$::POA neurons does not increase anxiety-like behaviors (**Figure 6)**, which may be important to permit flexible selection of specific active coping behaviors. Further, SuM$^{VGLUT2+}$::POA neurons do not appear to evoke stereotyped or compulsive behaviors described for other threat response behaviors, such as the flee and freeze behavior evoked by activation neurons in the superior colliculus(79). Our results obtained using an operant task confirmed that that photostimulation of SuM$^{VGLUT2+}$::POA neurons encodes aversiveness, potentially associated with a stressor, and can function as a negative reinforcer. Supporting a role for SuM$^{VGLUT2+}$::POA neurons in mediating flexible active coping behaviors, the results demonstrated that photostimulation was sufficient to drive active action-outcome behaviors (i.e., nose port activation) and that performance of the task was rapidly learned and performed during photostimulation(**Figure 8**). Superficially, our finding of the aversiveness of SuM$^{VGLUT2+}$::POA neuron contrasts with a recent study that found photostimulation of SuM neurons projections could be reinforcing. However, in the same study photostimulation of projections from SuM to the septum drove place preference (septum) but in photostimulation of SuM projections in the PV was aversive (PV) (19). We report here that SuM$^{VGLUT2+}$::POA neurons also project to the PV and the septum (**Figure 2**). A plausible interpretation is that SuM contains separable populations of neurons which gate a host of distinct behavioral strategies. One set (PV projecting) can drive aversion and the other (non-PV projecting) regulate reinforcement. Although delineating the overarching circuitry will require further studies, our results and together with recent studies establish that SuM is an important and poorly understood node for regulating appetitive and aversive motivated behaviors.

The results presented here indicate a previously unrecognized role for SuM$^{VGLUT2+}$::POA neurons as an important node for shifting behavioral control to active coping strategies. In the absence of external stressors, photostimulation of SuM$^{VGLUT2+}$::POA evoked escape and defensive burying behaviors (**Figure 5**), both active coping strategies. Forced swim test offers an

ongoing unescapable stressor that can be addressed using both passive and active coping strategies, with passive behaviors increasing with time in the test (47, 80). During the second day of forced swim, when passive behavior (immobility) predominated, photostimulation of SuM$^{VGLUT2+}$::POA neurons was sufficient to drive a potent switch to active coping behavior with decreased time immobile and increased swimming and wall climbing (**Figure 8B and C**). Surprisingly, a short bout of photostimulation produced an increase in active coping behavior that exceeded the time of photostimulation. The extended effect of photostimulation was also evident in other assays and manifested often as increased grooming behavior alongside (**Figure 5**) suppression of feeding (**Figure 8**). In food deprived mice, photostimulation of SuM$^{VGLUT2+}$::POA neurons was sufficient to redirect behavior away from feeding. Ethologically, mice must choose rapidly between threat and feeding, implicating this pathway in direct control of immediate switching between these behaviors.

Our results expand the understanding of functional and neurochemical diversity within the SuM, particularly with respect to projections to hippocampus(21, 24, 81). Further evidence for functional diversity in SuM is found in a recent study that separates SuM neurons based on Tac1 expression, reporting that Tac1+ but not Tac1- neuronal activity correlated with future velocity and when activated evoked locomotor activity(41). Relevant to our findings, the Tac1 expressing neurons implicated in encoding velocity projected to the DG, while SuM$^{VGLUT2+}$::POA do not (**Figure 3**) indicating that they are likely to be a separable population. Furthermore, we observed that stimulation of SuM$^{VGLUT2+}$::POA neurons evoked a range of behaviors not limited to increased speed of travel. Stimulation of SuM$^{VGLUT2+}$::POA neurons also drove high performance of a negative reinforcement task that would have been precluded by forced stereotypic locomotor activity. Taken together, our study shows that SuM is a critical network node with functional diversity among neuronal populations that plays important roles in regulating active coping behaviors.

Another important function ascribed to SuM is regulation of arousal(23). How SuM$^{VGLUT2+}$::POA neurons relate to arousal promoting roles of VGLUT+ SuM neurons is currently unclear. The projections to the POA, which contains wake promoting neurons including neurons in the LPO, makes this an appealing population to be involved in wakefulness(25, 26). The SuM population implicated in arousal is also VGAT- and VGLUT2+(23). However, photoactivation of SuM projections in the dentate gyrus, which does not receive projections from SuM$^{VGLUT2+}$::POA neurons, triggered wakefulness from slow wave sleep(21). Understanding how the newly appreciated neural populations in SuM relate to each other and which population(s) are involved in arousal will require additional high-resolution approaches and a thorough investigation.

SuM$^{VGLUT2+}$::POA neurons may also be functionally related to nearby neurons. SuM$^{VGLUT2+}$::POA neurons are anatomically separate from but are in proximity to the ventral tegmental area. Prior reports on glutamatergic neurons in the VTA identified cells that respond to aversive stimuli and drive aversion and promote innate defensive behaviors(82-84). Slightly rostral and lateral to SuM is the dorsal premammillary nucleus. Cholecystokinin expressing neurons in the dorsal premammillary nucleus were reported to be for escape behaviors through input to the PAG(85). Functional magnetic resonance imaging studies in humans has shown that aversive stimuli cause increased covariation of BOLD signal in the posterior hypothalamus and PAG (86). Given the anatomical proximity of dorsal premammillary nucleus to SuM, neurons in SuM are also potentially implicated in aversive processing found in these fMRI studies. Lesion studies have identified roles in threat response for dorsal premammillary nucleus and SuM (14, 87). Understanding how the SuM$^{VGLUT2+}$::POA neurons may connected with, functionally related to, or share a common identity with the dorsal premammillary or VGLUT+ VTA populations will be important and interesting follow-up investigations.

In conclusion, we have identified a population of VGLUT2+ neurons in SuM (SuM$^{VGLUT2+}$::POA) that arborize with projections to multiple areas involved in regulation of stress coping and threat response behaviors. We determined that SuM$^{VGLUT2+}$::POA neurons represent a distinct population that is activated by acute stressors. Furthermore, we report that SuM$^{VGLUT2+}$::POA neurons drive aversion and evokes active coping behaviors while suppressing feeding. This study implicates SuM$^{VGLUT2+}$::POA neurons as a key circuit which responds to threats and stressors and may play important roles in determining risk for stress-dependent neuropsychiatric disorders.

Acknowledgements

This work was supported by the NIH through 5R01MH112355 to MRB and 5K08MH119538 to AJN. Support was also provided by the Hope Center Viral Vectors Core and the Genome Technology Resource Center at Washington University in St. Louis (NIH P30CA91842 and UL1TR000448). This work was supported by a Pilot Project Award from the Hope Center for Neurological Disorders and by the Hope Center Viral Vectors Core at Washington University School of Medicine.

Materials and Methods

STAR methods

Key Resources Table:

Reagent type (species) or resource	Source or reference	Identifiers
Antibodies		
Alexa Fluor 488 Goat anti-Rabbit IgG	Invitrogen	Cat# A11008
Phospho-c-Fos (Ser32) (D82C12) XP®	Cell Signaling Technology	Cat# 5348
Chemicals		
4% paraformaldehyde	J.T. Baker, Avantor	S898-09
Goat Serum	Sigma Aldrich	G9023
Vectashield Hardset Antifade Mounting Medium With DAPI	Vector Laboratories	Cat# NC9029229
Experimental Models: Organisms/Strains		
Slc17a6tm2(cre)Lowl/J (VGLUT2-Cre)	The Jackson Laboratory	RRID:IMSR_JAX:016963
B6;129S-Slc17a6tm1.1(flpo)Hze/J (VGLUT2-Flp)	The Jackson Laboratory	RRID: IMSR_JAX: 030212
Mouse:B6.Cg-*Gt(ROSA)26Sor*$^{tm14(CAG-tdTomato)Hze}$/J (Ai14)	The Jackson Laboratory	RRID: IMSR_JAX: 007914
B6J.129S6(FVB)-*Slc32a1*$^{tm2(cre)Lowl}$/MwarJ (VGAT-Cre)	The Jackson Laboratory	RRID: IMSR_JAX: 028862
C57BL/6J	The Jackson Laboratory	RRID: IMSR_JAX: 000664
Bacterial and Virus Strains		
AAV5-EF1a-DIO-hChR2(H134R)-EYFP (2.5 × 10^{13} vg/ml)	Washington University Hope Center Viral Vector Core	N/A
AAV2-Retro-DIO-ChR2-eYFP (2.8 × 10^{12} vg/ml)	Washington University Hope Center Viral Vector Core	N/A
AAV2-retro-FLEX-tdTomato (7 × 10^{12} vg/ml)	Addgene	RRID: Addgene_ 28306-AAVrg

AAV5-DIO-ChR2-eYFP (1.4 × 10^{13} vg/ml)	Washington University Hope Center Viral Vector Core	N/A
AAV2-Retro-EF1a-fDIO-cre (7 × 10^{12} vg/ml)	Addgene	RRID: Addgene_ 121675-AAVrg
AAV2-EF1a-Nuc-flox(mCherry)-EGFP (5 × 10^{12} vg/ml)	Addgene	RRID: Addgene_112677-AAV5
Retro-AAV2-EF1a-Nuc-flox(mCherry)-EGFP	Addgene	RRID: Addgene_ 112677-AAVrg
AAV2-retro-EF1a-DIO-eYFP (3 × 10^{13} vg/ml)	Washington University Hope Center Viral Vector Core	N/A
AAV-retro-EF1a-Flpo (1.02 × 10^{13} GC/mL or 7 × 10^{12} vg/ml)	Addgene	RRID: Addgene_ 55637-AAVrg
AAV9-EF1a-fDIO-cre (2.5 × 10^{13} GC/mL or 1 × 10^{13} vg/ml)	Addgene	RRID: Addgene_121675-AAV9
Retro-AAV2-EF1a-Cre (2.1 × 10^13 GC/mL)	Addgene	RRID: Addgene_55636-AAVrg
AAV9-syn-FLEX-GCaMP7s-WPRE	Addgene	Addgene_104487-AAV9
Software		
Bonsai	Bonsai-rx.org	N/A
Ethovision	Noldus	N/A
GraphPad Prism	GraphPad Software	N/A

Contact for reagent and resource sharing

For further information regarding reagents and resources, contact Aaron Norris, norrisa@wustl.edu.

Experimental model and subject details

Adult (25-35 g, at least 8 weeks of age upon experimental use) male and female VGLUT-Cre (RRID: IMSR_JAX:016963), VGLUT2-Flp (RRID: IMSR_JAX: 030212), Ai14 (RRID: IMSR_JAX: 007908), VGAT-Cre (RRID: IMSR_ JAX: 028862) and C57BL/6J (RRID: IMSR_JAX: 000664) mice (species *Mus musculus*) were group housed (no more than five littermates per cage) in a 12 hr:12 hr light:dark cycle room with food and water ad libitum(88). The Washington

University Animal Care and Use Committee approved all procedures, which adhered to NIH guidelines.

Stereotaxic surgery

Injections and implantations were done as described previously(34, 89). Briefly, in an induction chamber, mice were anesthetized (4% isoflurane) before being placed in a stereotaxic frame (Kopf Instruments). Anesthesia was maintained with 2% isoflurane. Mice were then injected unilaterally or bilaterally, depending on the combination of virus(es) used and brain regions injected. A blunt needle Neuros Syringe (65457-01, Hamilton Con.) and syringe pump (World Precision Instruments) were used to perform the injection schemes below. After surgery, a warmed recovery chamber housed the animal while it recovered from anesthesia before being returned to its home cage.

Virus	Virus Volume	Brain region/coordinates
AAV5-EF1a-DIO-hChR2(H134R)-EYFP		Region, laterality, (AP , ML , DV)
AAV2-retro-DIO-ChR2-eYFP	100 nl	
AAV2-retro-FLEX-tdTomato	100 nl	Septum (AP +0.9, ML +0.3, DV -3.5) LPAG, unilateral (AP -4.65, ML +0.6, DV -2.85)
AAV5-DIO-ChR2-eYFP		
AAV2-retro-EF1a-fDIO-cre	100 nl	POA, bilateral (AP +0.45, ML ± 0.5, DV -5.35)
AAV2-EF1a-Nuc-flox(mCherry)-EGFP	300 nl	SuM (AP -2.7, ML +0.05, DV -4.3)
AAV2-retro-EF1a-Nuc-flox(mCherry)-EGFP	150 nl	POA, bilateral (AP +0.45, ML ± 0.5, DV -5.35)
AAV22-retro-EF1a-DIO-eYFP	100 nl	Acb (AP +1.4, +0.6 ML, DV -4.75) POA, bilateral (AP +0.45, ML ± 0.5, DV -5.35)
AAV2-retro-EF1a-Flpo	50 nl	POA, bilateral (AP +0.45, ML ± 0.5, DV -5.35)
AAV9-EF1a-fDIO-cre	100 nl 50 nl	SuM (AP -2.7, ML +0.05, DV -4.3)

Injections were made at a rate of 50 nl/min, with the injection needle being withdrawn 5 min after the end of the infusion. Fiber optics for photostimulation or optical fibers for fiber

photometry were implanted after injections for all behavioral experiments. Fiber optics for photostimulation or optical fibers for fiber photometry were implanted after injections for all behavioral experiments.

Fiber optic implants for photostimulation were fabricated as previously described using 200µm glass fibers and implanted midline over SuM (34, 90). For implantation, the skull was cleaned and etched with OptiBond® (Kerr) and the fiber was cemented to the skull with Tetric N-Flow® (Ivoclar Vivadent). Blue light was used to cure and harden cement. Mice were allowed to recover for at least seven days before the start of behavioral experiments. The same process was used for implantation for fiber photometry fibers, which were trimmed to length (NeuroPhotometrics).

Anatomical tracing

For anterograde viral tracing experiments, virus (was injected at least six weeks prior to transcardial perfusions with 4% paraformaldehyde to allow for anterograde transport of the fluorophore. AAV5-EF1a-DIO-hChR2eYFP or AAV5-EF1a-DIO-eYFP were used. Alternatively, to label only $SuM^{VGLUT2+}$::POA neurons for anterograde tracing Retro-AAV2-DIO-eYFP or Retro-DIO-ChR21eYFP was injected into the POA with AAV-fDIO-Cre injected in the SuM. A minimum of 6 weeks was allowed prior to sacrifice, harvesting or brains, and sectioning (30µM). Serial 30 µM sections approximately 60µM apart were examined. For retrograde studies viruses were injected (see figure legends and text for specific viruses) at the targeted site and table for specific viruses(40, 55, 91). Three weeks were allowed to elapse prior to harvesting brains following injections. Images were obtained on a Leica DM6 B upright microscope and a processed using Thunder imaging station (Leica).

Brain clearing and light sheet miscopy

Tissue clearing and imaging was carried out on brains collected and fixed in 4% PFA as described above by LifeCanvas Technologies. Briefly, brains were fixed using SHIELD post ix and cleared for 7 days in SmartClear II Pro. Index matched with EASYIndex at room temperature. Samples were mounted ventral side up and imaged at 3.6x with pixel size 1.8 x 1.8 mm, axial resolution < 4 µm, z step 4 µm in 488nm channel. Fos was labeled by Alexa Flour 488. SuM boundaries were defined by -2.6 to -2.95 rostral to Bregma. The medial mammillary nucleus and the mammillary recess of the 3rd ventricle marked the medial and ventral boundaries while fornix marked the lateral, and fasciculus retroflexus the dorsal boundaries. Images were quantified by a trained laboratory member who was blind to the experimental conditions.

Immunohistochemistry

Mice were intracardially perfused with 4% PFA and then brains were sectioned (30 microns) and placed in 1x PB until immunostaining. Free-floating sections were washed in 3 times in 1x PBS for 10 min intervals. Sections were then placed in blocking buffer (0.5% Triton X-100% and 5% natural goat serum in 1z PBS) for 1 hr at room temperature. After blocking buffer, sections were placed in primary antibody rabbit Phospho-c-Fos (Ser32) antibody (1:500, Cell Signaling Technology) overnight 4° C temperature. After 3 x 10 min 1x PBS washes, sections were incubated in secondary antibody goat anti-rabbit Alexa Fluor 488 (1:2500, Invitrogen) for 2 hr at room temperature. Sections were washed in 1x PBS (3 x 10 min) followed by 2 x 10 min 1x PB washes. After immunostaining, sections were mounted on Super Frost Plus slides (Fisher) and covered with Vectashield Hard set mounting medium with DAPI (RRID:AB_2336788, Vector Laboratories) and cover glass prior to being imaged.

Imaging and cell quantification

'The Mouse Brain in Stereotaxic Coordinates' provided the framework to label brain sections relative to bregma(92). A Leica DM6 B epifluorescent microscope was used to image all

sections. For eYFP visualization, a YFP filter cube (Excitation: 490-510, Dichroic: 515, Emission: 520-550) was used and for tdTomato visualization, a Texas Red Filter Cube (Excitation: BP 560/40, Dichroic: LP 585, Emission: BP 630/75) was used. Fos was labeled by Alexa Flour 488. SuM boundaries were defined by -2.6 to -2.95 rostral to Bregma. The medial mammillary nucleus and the mammillary recess of the 3rd ventricle marked the medial and ventral boundaries while fornix marked the lateral, and fasciculus retroflexus the dorsal boundaries. Images were quantified by a trained laboratory member who was blind to the experimental conditions

Forced-Swim Test

For stress induction via forced swim (**Figure 4**)(47, 93), mice were individually placed in a cylindrical container (18 cm in diameter) filled with water at 25 +/- 1 ^{o}C for 15 min. Prior to stress force swimming, mice were habituated to the arenas for three days prior to the beginning of FST to minimize stress. Control mice were brought to the behavioral testing area but remained in the home cage until sacrifice. Water was replaced after every animal.

Fiber Photometry

Mice were injected bilaterally in POA with pAV-retro-EF1a-fDIO-cre and a midline injection with AAV-syn-FLEX-GCaMP7s-WPRE in SuM. After two weeks, mice were implanted with fiber-optic cannulas (200µm) in SuM (D/V -4.3-5)(48). Mice recovered a minimum of one week prior to behavioral testing. Recording of GCaMP and isosbestic were made using described methods using Bonsai software and FP3002 (Neurophotometrics)(94, 95). 470 and 415 nm LEDs were used to record interleaved isosbestic and GCaMP Ca2+ dependent signals following the manufactures directions.

For repeated forced swim experiments (dunk tank) mice placed inside a custom-made plastic rectangular enclosure (20 cm x 20cm x 23 cm) filled with water 30 +/- 1 ^{o}C. The enclosure

has a square wire mesh platform that could be raised and lowered without touching the animal. The platform was lowered for the swim session and raised at the conclusion of each session. During testing mice were tether to a fiberoptic patch cabled that was attached to a counter balanced arm that prevented downward force on the animal.

For foot shock stress testing, mice were individually placed inside a custom-made clear plastic box (15.24 L x 13.34 W x 14 H cm) inside a sound-attenuated cabinet. A speaker was placed 4 cm above the chamber for the delivery of auditory cues (75dB). A constant current aversive stimulator (ENV-414S) delivered foot shocks through a grid floor (0.7mA). Five shocks of 2 seconds were delivered after a 30 s tone. Intertrial interval ranged from 90 to 180 seconds. After the session, the animal was removed from the chamber and placed back in its home cage. The chamber and grid were wiped down with 70% ethanol between animals.

For fiber photometry data analysis, both the isosbestic and the GCaMP signals were preprocessed using a bandpass Butterworth filter (upper threshold: 6 Hz, lower threshold: 0.005 Hz) and then z-scores were calculated. The isosbestic signal was then subtracted from the GCaMP signals to control for motion artifacts.

For peri-event histograms analysis the follow workflow was used. For the shock experiments, a baseline window was used that went from 20 to 25 seconds after the beginning of the tone. The shock window went from 30 to 35 seconds after the beginning of the tone (0 to 5 seconds after the shock). For the forced swim trials, the baseline window went from -20 to -10 seconds, and the stimulus window went from 0 to 10 seconds

Real-time place aversion testing

For real-time place preference testing with optogenetic photostimulation we used custom-made, unbiased, balanced two-compartment conditioning apparatus (52.5 x 25.5 x 25.5 cm) as described previously(34, 89, 96). Mice were tethered to a patch cable that allowed free access to the entire arena for 30 min. Entry into one compartment triggered photostimulation, 1Hz, 5Hz, 10Hz, or 20 Hz (473 nm laser, 10 ms pulse width) that persisted while the mouse remained in the

light paired side. The side paired with photostimulation was counterbalanced across mice. Ordering was counterbalanced with respect to stimulation frequency and placement. Bedding in the behavior apparatus was replaced between every trial, and the floors and walls of the apparatus were wiped down with 70% ethanol. Time spent in each chamber and total distance traveled for the entire 30-minute trial was measured using Ethovision 10 (Noldus Information Technologies).

Light /Dark choice

For light/dark choice the same areas as used for real time preference testing were modified and used as previously described (97). On the light side a small sport light was placed overhead, and the walls cover with white laminated paper. Light levels on this side measure 580-590 lux. For the dark side, an infrared spotlight was placed over head, to allow for video tracking of the mice. The walls were covered with matte black plastic. Light levels in the center of the dark side measure 100-110 lux. Animals were recorded using a USB web cam without an infrared filter. For real-time aversion testing photostimulation was paired with the dark side of arena as described above. For anxiety-like behavior testing stimulation was provided uniformly during the trials. Time spent in each chamber and total distance traveled for the entire 30-minute trial was measured using Ethovision 10.

Observational behavioral assay

To observe behaviors evoked by photostimulation of $SuM^{VGLUT2+}$::POA neurons we mice were habituated for at least 3 days prior to testing to round (18 cm diameter) clear arena with counterbalanced optical commutators to minimize impact of the head tether on movement. Testing occurred after habitation and approximately 2 cm of bedding material was placed in arena. Behavior was record from the side and scored by a blinded observer.

Negative reinforcer two nose port operant behavior testing

For operant behavior testing we used Med Associates mouse operant conditioning chamber with dual nose ports and house light as previously described(95). Briefly, mice were tethered via cantilevered counterweighted optical commutator to a laser light source. A five-day protocol call was used. Day one through four were 10-minute trials. Photostimulation was provided at 10 Hz and activation of the active port resulted in a 10-second pause in the photostimulation and activation of the house light inside the arena. On the first four days each activation of the active port outside of a 10-second paused resulted in a new pause. On day five was a 30-minute trial using a progressive ratio protocol the number activation of the active port to generate a pause increased with each activation based on the $number\ of\ activations\ (j) = [5e^{(0.2j)} - 5]$ round to the nearest integer generating the schedule 1, 2, 4, 6, 9, 12, 15, 20, 25, 32, 40, 50….(98). Photostimulation terminated at the conclusion of the trial.

Forced Swim with photostimulation

Forced swim trials with optogenetic stimulation were done as a two-day test. On the first day all mice were subjected to a 15-minute forced swim, dried and return the home cage. On the second day they were tethered and subjected to a 6-minute forced swim divided into three periods, each two minutes in length, pre stimulation, stimulation, and post stimulation. 10 Hz photostimulation was provided during the trial. Mice were closely monitored during each trial of swimming. Trials were recorded and scored by a blinded observer for time spent immobile on the second day of the test.

Feeding after food deprivation

For tests involving brief access to food after deprivation, the same 18 cm diameter round arenas with counter balanced optical commutators were used. Mice were a habituated to the arenas for a minimum 3 days prior to testing. Mice were food deprived by removal of food from the home cage 24 hours prior to testing. Mice were placed in the arena and allowed to habituate

prior to introduction of a chow pellet. The 20-minutue trial with the foot pellet was recorded and scored by a blinded observer. Chow pellets were weighed before and after the 20-min trial. The difference is reported as food eaten.

Open field Test

For Open Field testing we used a purpose-built 20in square behavior arena. Mice were tethered to a patch cable and placed into the behavioral arena. The laser frequency was set to 10 Hz and was left on for 20 minutes. Distance moved for the 20-minute trial was quantified using Ethovision 10. Bedding in the arena was replaced between every trial, and the floors and walls of the arena were wiped down with 70% ethanol

Statistical analyses

Statistical analyses were conducted using GraphPad Prism software. Data are shown as mean ±SEM except for z-scores which as shown as ± 95% confidence interval, as noted in text. Values for individual p values are given in the text and figure legends. Significance was held at α less than 0.05. Unless noted in the test, nonparametric Mann-Whitney tests were used for statistical comparisons. In cases of multiple comparisons, Holm-Šídák method was used to correct for multiple comparisons. Paired testing was used with comparing within cohorts with repeated measurements and unpaired between cohorts. All “n” values represent the number of animals in a particular group for an experiment. For fiber photometry statistical analysis, the mean signal of the baseline and stimulus windows was used, and comparisons were made using the Wilcoxon ranked-sum test, with α=0.95

1. LeDoux J, Daw ND. Surviving threats: neural circuit and computational implications of a new taxonomy of defensive behaviour. Nat Rev Neurosci. 2018;19(5):269-82. Epub 2018/03/30. doi: 10.1038/nrn.2018.22. PubMed PMID: 29593300.
2. LeDoux JE. Coming to terms with fear. Proc Natl Acad Sci U S A. 2014;111(8):2871-8. Epub 2014/02/07. doi: 10.1073/pnas.1400335111. PubMed PMID: 24501122; PMCID: PMC3939902.
3. Mobbs D, Hagan CC, Dalgleish T, Silston B, Prevost C. The ecology of human fear: survival optimization and the nervous system. Front Neurosci. 2015;9:55. Epub 2015/04/09. doi: 10.3389/fnins.2015.00055. PubMed PMID: 25852451; PMCID: PMC4364301.
4. Shin LM, Liberzon I. The neurocircuitry of fear, stress, and anxiety disorders. Neuropsychopharmacology. 2010;35(1):169-91. Epub 2009/07/25. doi: 10.1038/npp.2009.83. PubMed PMID: 19625997; PMCID: PMC3055419.
5. Ressler KJ, Mayberg HS. Targeting abnormal neural circuits in mood and anxiety disorders: from the laboratory to the clinic. Nat Neurosci. 2007;10(9):1116-24. Epub 2007/08/30. doi: 10.1038/nn1944. PubMed PMID: 17726478; PMCID: PMC2444035.
6. Kessler RC, Angermeyer M, Anthony JC, R DEG, Demyttenaere K, Gasquet I, G DEG, Gluzman S, Gureje O, Haro JM, Kawakami N, Karam A, Levinson D, Medina Mora ME, Oakley Browne MA, Posada-Villa J, Stein DJ, Adley Tsang CH, Aguilar-Gaxiola S, Alonso J, Lee S, Heeringa S, Pennell BE, Berglund P, Gruber MJ, Petukhova M, Chatterji S, Ustun TB. Lifetime prevalence and age-of-onset distributions of mental disorders in the World Health Organization's World Mental Health Survey Initiative. World Psychiatry. 2007;6(3):168-76. Epub 2008/01/12. PubMed PMID: 18188442; PMCID: PMC2174588.
7. Southwick SM, Vythilingam M, Charney DSJARCP. The psychobiology of depression and resilience to stress: implications for prevention and treatment2005;1:255-91.
8. Ledoux JE, Gorman JM. A call to action: Overcoming anxiety through active coping. Am J Psychiat. 2001;158(12):1953-5. doi: DOI 10.1176/appi.ajp.158.12.1953. PubMed PMID: WOS:000172452100001.
9. Steimer T. Animal models of anxiety disorders in rats and mice: some conceptual issues. Dialogues Clin Neurosci. 2011;13(4):495-506. Epub 2012/01/26. PubMed PMID: 22275854; PMCID: PMC3263396.
10. Penzo MA, Robert V, Tucciarone J, De Bundel D, Wang M, Van Aelst L, Darvas M, Parada LF, Palmiter RD, He M, Huang ZJ, Li B. The paraventricular thalamus controls a central amygdala fear circuit. Nature. 2015;519(7544):455-9. Epub 2015/01/21. doi: 10.1038/nature13978. PubMed PMID: 25600269; PMCID: PMC4376633.
11. Ma J, du Hoffmann J, Kindel M, Beas BS, Chudasama Y, Penzo MA. Divergent projections of the paraventricular nucleus of the thalamus mediate the selection of passive and active defensive behaviors. Nat Neurosci. 2021;24(10):1429-40. Epub 2021/08/21. doi: 10.1038/s41593-021-00912-7. PubMed PMID: 34413514; PMCID: PMC8484052.
12. Gross CT, Canteras NS. The many paths to fear. Nat Rev Neurosci. 2012;13(9):651-8. Epub 2012/08/02. doi: 10.1038/nrn3301. PubMed PMID: 22850830.
13. Amorapanth P, LeDoux JE, Nader K. Different lateral amygdala outputs mediate reactions and actions elicited by a fear-arousing stimulus. Nat Neurosci. 2000;3(1):74-9. PubMed PMID: WOS:000085810200015.
14. Canteras NS, Chiavegatto S, Ribeiro do Valle LE, Swanson LW. Severe reduction of rat defensive behavior to a predator by discrete hypothalamic chemical lesions. Brain Res Bull. 1997;44(3):297-305. Epub 1997/01/01. doi: 10.1016/s0361-9230(97)00141-x. PubMed PMID: 9323445.
15. Pan WX, McNaughton N. The supramammillary area: its organization, functions and relationship to the hippocampus. Prog Neurobiol. 2004;74(3):127-66. Epub 2004/11/24. doi: 10.1016/j.pneurobio.2004.09.003. PubMed PMID: 15556285.

16. Vertes RP, McKenna JT. Collateral projections from the supramammillary nucleus to the medial septum and hippocampus. Synapse. 2000;38(3):281-93. doi: Doi 10.1002/1098-2396(20001201)38:3<281::Aid-Syn7>3.0.Co;2-6. PubMed PMID: WOS:000089993400007.
17. Vertes RP. Pha-L Analysis of Projections from the Supramammillary Nucleus in the Rat. J Comp Neurol. 1992;326(4):595-622. doi: DOI 10.1002/cne.903260408. PubMed PMID: WOS:A1992KC85400007.
18. Kiss J, Csaki A, Bokor H, Kocsis K, Kocsis B. Possible glutamatergic/aspartatergic projections to the supramammillary nucleus and their origins in the rat studied by selective [(3)H]D-aspartate labelling and immunocytochemistry. Neuroscience. 2002;111(3):671-91. Epub 2002/05/29. doi: 10.1016/s0306-4522(02)00037-4. PubMed PMID: 12031353.
19. Kesner AJ, Shin R, Calva CB, Don RF, Junn S, Potter CT, Ramsey LA, Abou-Elnaga AF, Cover CG, Wang DV, Lu H, Yang Y, Ikemoto S. Supramammillary neurons projecting to the septum regulate dopamine and motivation for environmental interaction in mice. Nat Commun. 2021;12(1):2811. Epub 2021/05/16. doi: 10.1038/s41467-021-23040-z. PubMed PMID: 33990558; PMCID: PMC8121914.
20. Li Y, Bao H, Luo Y, Yoan C, Sullivan HA, Quintanilla L, Wickersham I, Lazarus M, Shih YI, Song J. Supramammillary nucleus synchronizes with dentate gyrus to regulate spatial memory retrieval through glutamate release. Elife. 2020;9. Epub 2020/03/14. doi: 10.7554/eLife.53129. PubMed PMID: 32167473; PMCID: PMC7069722.
21. Billwiller F, Castillo L, Elseedy H, Ivanov AI, Scapula J, Ghestem A, Carponcy J, Libourel PA, Bras H, Abdelmeguid NE, Krook-Magnuson E, Soltesz I, Bernard C, Luppi PH, Esclapez M. GABA-glutamate supramammillary neurons control theta and gamma oscillations in the dentate gyrus during paradoxical (REM) sleep. Brain Struct Funct. 2020;225(9):2643-68. Epub 2020/09/25. doi: 10.1007/s00429-020-02146-y. PubMed PMID: 32970253; PMCID: PMC7674372.
22. Ito HT, Moser EI, Moser MB. Supramammillary Nucleus Modulates Spike-Time Coordination in the Prefrontal-Thalamo-Hippocampal Circuit during Navigation. Neuron. 2018;99(3):576-87 e5. Epub 2018/08/10. doi: 10.1016/j.neuron.2018.07.021. PubMed PMID: 30092214.
23. Pedersen NP, Ferrari L, Venner A, Wang JL, Abbott SBG, Vujovic N, Arrigoni E, Saper CB, Fuller PM. Supramammillary glutamate neurons are a key node of the arousal system. Nat Commun. 2017;8. doi: ARTN 1405

10.1038/s41467-017-01004-6. PubMed PMID: WOS:000414869200004.
24. Leranth C, Kiss J. A population of supramammillary area calretinin neurons terminating on medial septal area cholinergic and lateral septal area calbindin-containing cells are aspartate/glutamatergic. J Neurosci. 1996;16(23):7699-710. Epub 1996/12/01. PubMed PMID: 8922426; PMCID: PMC6579088.
25. Swanson LJBrb. The projections of the ventral tegmental area and adjacent regions: a combined fluorescent retrograde tracer and immunofluorescence study in the rat1982;9(1-6):321-53.
26. Kocsis K, Kiss J, Csaki A, Halasz B. Location of putative glutamatergic neurons projecting to the medial preoptic area of the rat hypothalamus. Brain Res Bull. 2003;61(4):459-68. Epub 2003/08/12. doi: 10.1016/s0361-9230(03)00180-1. PubMed PMID: 12909290.
27. Pan W-X, McNaughton NJPin. The supramammillary area: its organization, functions and relationship to the hippocampus2004;74(3):127-66.
28. Soussi R, Zhang N, Tahtakran S, Houser CR, Esclapez MJEJoN. Heterogeneity of the supramammillary–hippocampal pathways: Evidence for a unique GABAergic neurotransmitter phenotype and regional differences2010;32(5):771-85.
29. Reitz SL, Wasilczuk AZ, Beh GH, Proekt A, Kelz MB. Activation of Preoptic Tachykinin 1 Neurons Promotes Wakefulness over Sleep and Volatile Anesthetic-Induced Unconsciousness. Curr Biol.

2021;31(2):394-405 e4. Epub 2020/11/15. doi: 10.1016/j.cub.2020.10.050. PubMed PMID: 33188746; PMCID: PMC7855813.
30. Yamagata T, Kahn MC, Prius-Mengual J, Meijer E, Sabanovic M, Guillaumin MCC, van der Vinne V, Huang YG, McKillop LE, Jagannath A, Peirson SN, Mann EO, Foster RG, Vyazovskiy VV. The hypothalamic link between arousal and sleep homeostasis in mice. Proc Natl Acad Sci U S A. 2021;118(51). Epub 2021/12/15. doi: 10.1073/pnas.2101580118. PubMed PMID: 34903646; PMCID: PMC8713782.
31. Szymusiak R, Alam N, Steininger TL, McGinty D. Sleep-waking discharge patterns of ventrolateral preoptic/anterior hypothalamic neurons in rats. Brain Res. 1998;803(1-2):178-88. Epub 1998/09/05. doi: 10.1016/s0006-8993(98)00631-3. PubMed PMID: 9729371.
32. Nollet M, Wisden W, Franks NP. Sleep deprivation and stress: a reciprocal relationship. Interface Focus. 2020;10(3):20190092. Epub 2020/05/10. doi: 10.1098/rsfs.2019.0092. PubMed PMID: 32382403; PMCID: PMC7202382.
33. McGinty D, Szymusiak R. Hypothalamic regulation of sleep and arousal. Front Biosci. 2003;8:s1074-83. Epub 2003/09/06. PubMed PMID: 12957869.
34. Norris AJ, Shaker JR, Cone AL, Ndiokho IB, Bruchas MR. Parabrachial opioidergic projections to preoptic hypothalamus mediate behavioral and physiological thermal defenses. Elife. 2021;10. doi: ARTN e60779

10.7554/eLife.60779. PubMed PMID: WOS:000626459000001.
35. Barker DJ, Miranda-Barrientos J, Zhang SL, Root DH, Wang HL, Liu B, Calipari ES, Morales M. Lateral Preoptic Control of the Lateral Habenula through Convergent Glutamate and GABA Transmission. Cell Rep. 2017;21(7):1757-69. doi: 10.1016/j.celrep.2017.10.066. PubMed PMID: WOS:000415073200006.
36. Nakamura K, Nakamura Y, Kataoka N. A hypothalamomedullary network for physiological responses to environmental stresses. Nat Rev Neurosci. 2022;23(1):35-52. Epub 2021/11/04. doi: 10.1038/s41583-021-00532-x. PubMed PMID: 34728833.
37. Haglund L, Swanson LW, Kohler C. The Projection of the Supramammillary Nucleus to the Hippocampal-Formation - an Immunohistochemical and Anterograde Transport Study with the Lectin Pha-L in the Rat. J Comp Neurol. 1984;229(2):171-85. doi: DOI 10.1002/cne.902290204. PubMed PMID: WOS:A1984TP17000002.
38. Hayakawa T, Ito H, Zyo K. Neuroanatomical Study of Afferent-Projections to the Supramammillary Nucleus of the Rat. Anat Embryol. 1993;188(2):139-48. PubMed PMID: WOS:A1993LR28100003.
39. Hashimotodani Y, Karube F, Yanagawa Y, Fujiyama F, Kano M. Supramammillary Nucleus Afferents to the Dentate Gyrus Co-release Glutamate and GABA and Potentiate Granule Cell Output. Cell Rep. 2018;25(10):2704-15 e4. Epub 2018/12/06. doi: 10.1016/j.celrep.2018.11.016. PubMed PMID: 30517859.
40. Back S, Necarsulmer J, Whitaker LR, Coke LM, Koivula P, Heathward EJ, Fortuno LV, Zhang Y, Yeh CG, Baldwin HA, Spencer MD, Mejias-Aponte CA, Pickel J, Hoffman AF, Spivak CE, Lupica CR, Underhill SM, Amara SG, Domanskyi A, Anttila JE, Airavaara M, Hope BT, Hamra FK, Richie CT, Harvey BK. Neuron-Specific Genome Modification in the Adult Rat Brain Using CRISPR-Cas9 Transgenic Rats. Neuron. 2019;102(1):105-19 e8. Epub 2019/02/23. doi: 10.1016/j.neuron.2019.01.035. PubMed PMID: 30792150.
41. Farrell JS, Lovett-Barron M, Klein PM, Sparks FT, Gschwind T, Ortiz AL, Ahanonu B, Bradbury S, Terada S, Oijala M, Hwaun E, Dudok B, Szabo G, Schnitzer MJ, Deisseroth K, Losonczy A, Soltesz I. Supramammillary regulation of locomotion and hippocampal activity. Science. 2021;374(6574):1492-6. Epub 2021/12/17. doi: 10.1126/science.abh4272. PubMed PMID: 34914519.

42. Park YG, Sohn CH, Chen R, McCue M, Yun DH, Drummond GT, Ku T, Evans NB, Oak HC, Trieu W, Choi H, Jin X, Lilascharoen V, Wang J, Truttmann MC, Qi HW, Ploegh HL, Golub TR, Chen SC, Frosch MP, Kulik HJ, Lim BK, Chung K. Protection of tissue physicochemical properties using polyfunctional crosslinkers. Nat Biotechnol. 2018. Epub 2018/12/18. doi: 10.1038/nbt.4281. PubMed PMID: 30556815; PMCID: PMC6579717.
43. Madisen L, Zwingman TA, Sunkin SM, Oh SW, Zariwala HA, Gu H, Ng LL, Palmiter RD, Hawrylycz MJ, Jones AR, Lein ES, Zeng H. A robust and high-throughput Cre reporting and characterization system for the whole mouse brain. Nat Neurosci. 2010;13(1):133-40. Epub 2009/12/22. doi: 10.1038/nn.2467. PubMed PMID: 20023653; PMCID: PMC2840225.
44. Day HE, Masini CV, Campeau S. The pattern of brain c-fos mRNA induced by a component of fox odor, 2,5-dihydro-2,4,5-trimethylthiazoline (TMT), in rats, suggests both systemic and processive stress characteristics. Brain Res. 2004;1025(1-2):139-51. Epub 2004/10/07. doi: 10.1016/j.brainres.2004.07.079. PubMed PMID: 15464754.
45. Santin LJ, Aguirre JA, Rubio S, Begega A, Miranda R, Arias JL. c-Fos expression in supramammillary and medial mammillary nuclei following spatial reference and working memory tasks. Physiol Behav. 2003;78(4-5):733-9. Epub 2003/06/05. doi: 10.1016/s0031-9384(03)00060-x. PubMed PMID: 12782230.
46. Costa AP, Vieira C, Bohner LO, Silva CF, Santos EC, De Lima TC, Lino-de-Oliveira C. A proposal for refining the forced swim test in Swiss mice. Prog Neuropsychopharmacol Biol Psychiatry. 2013;45:150-5. Epub 2013/05/15. doi: 10.1016/j.pnpbp.2013.05.002. PubMed PMID: 23665107.
47. Commons KG, Cholanians AB, Babb JA, Ehlinger DG. The Rodent Forced Swim Test Measures Stress-Coping Strategy, Not Depression-like Behavior. ACS Chem Neurosci. 2017;8(5):955-60. Epub 2017/03/14. doi: 10.1021/acschemneuro.7b00042. PubMed PMID: 28287253; PMCID: PMC5518600.
48. Dana H, Sun Y, Mohar B, Hulse BK, Kerlin AM, Hasseman JP, Tsegaye G, Tsang A, Wong A, Patel R, Macklin JJ, Chen Y, Konnerth A, Jayaraman V, Looger LL, Schreiter ER, Svoboda K, Kim DS. High-performance calcium sensors for imaging activity in neuronal populations and microcompartments. Nat Methods. 2019;16(7):649-57. Epub 2019/06/19. doi: 10.1038/s41592-019-0435-6. PubMed PMID: 31209382.
49. De Boer SF, Koolhaas JM. Defensive burying in rodents: ethology, neurobiology and psychopharmacology. Eur J Pharmacol. 2003;463(1-3):145-61. Epub 2003/02/26. doi: 10.1016/s0014-2999(03)01278-0. PubMed PMID: 12600707.
50. Castro DC, Terry RA, Berridge KC. Orexin in Rostral Hotspot of Nucleus Accumbens Enhances Sucrose 'Liking' and Intake but Scopolamine in Caudal Shell Shifts 'Liking' Toward 'Disgust' and 'Fear'. Neuropsychopharmacology. 2016;41(8):2101-11. Epub 2016/01/21. doi: 10.1038/npp.2016.10. PubMed PMID: 26787120; PMCID: PMC4908641.
51. Reynolds SM, Berridge KC. Fear and feeding in the nucleus accumbens shell: rostrocaudal segregation of GABA-elicited defensive behavior versus eating behavior. J Neurosci. 2001;21(9):3261-70. Epub 2001/04/20. PubMed PMID: 11312311; PMCID: PMC6762573.
52. Richard JM, Berridge KC. Nucleus accumbens dopamine/glutamate interaction switches modes to generate desire versus dread: D(1) alone for appetitive eating but D(1) and D(2) together for fear. J Neurosci. 2011;31(36):12866-79. Epub 2011/09/09. doi: 10.1523/JNEUROSCI.1339-11.2011. PubMed PMID: 21900565; PMCID: PMC3174486.
53. Kalueff AV, Tuohimaa PJBRP. Grooming analysis algorithm for neurobehavioural stress research2004;13(3):151-8.
54. van Erp AM, Kruk MR, Meelis W, Willekens-Bramer DC. Effect of environmental stressors on time course, variability and form of self-grooming in the rat: handling, social contact, defeat, novelty, restraint and fur moistening. Behav Brain Res. 1994;65(1):47-55. Epub 1994/11/16. doi: 10.1016/0166-4328(94)90072-8. PubMed PMID: 7880454.

55. Lee JH, Durand R, Gradinaru V, Zhang F, Goshen I, Kim DS, Fenno LE, Ramakrishnan C, Deisseroth K. Global and local fMRI signals driven by neurons defined optogenetically by type and wiring. Nature. 2010;465(7299):788-92. Epub 2010/05/18. doi: 10.1038/nature09108. PubMed PMID: 20473285; PMCID: PMC3177305.
56. Kravitz AV, Tye LD, Kreitzer AC. Distinct roles for direct and indirect pathway striatal neurons in reinforcement. Nat Neurosci. 2012;15(6):816-8. Epub 2012/05/01. doi: 10.1038/nn.3100. PubMed PMID: 22544310; PMCID: PMC3410042.
57. McCall JG, Al-Hasani R, Siuda ER, Hong DY, Norris AJ, Ford CP, Bruchas MR. CRH Engagement of the Locus Coeruleus Noradrenergic System Mediates Stress-Induced Anxiety. Neuron. 2015;87(3):605-20. Epub 2015/07/28. doi: 10.1016/j.neuron.2015.07.002. PubMed PMID: 26212712; PMCID: PMC4529361.
58. Felix-Ortiz AC, Beyeler A, Seo C, Leppla CA, Wildes CP, Tye KM. BLA to vHPC inputs modulate anxiety-related behaviors. Neuron. 2013;79(4):658-64. Epub 2013/08/27. doi: 10.1016/j.neuron.2013.06.016. PubMed PMID: 23972595; PMCID: PMC4205569.
59. Jakovcevski M, Schachner M, Morellini F. Susceptibility to the long-term anxiogenic effects of an acute stressor is mediated by the activation of the glucocorticoid receptors. Neuropharmacology. 2011;61(8):1297-305. Epub 2011/08/09. doi: 10.1016/j.neuropharm.2011.07.034. PubMed PMID: 21820452.
60. Bailey KR, Crawley JN. Anxiety-Related Behaviors in Mice. In: nd, Buccafusco JJ, editors. Methods of Behavior Analysis in Neuroscience. Boca Raton (FL)2009.
61. Heredia L, Torrente M, Colomina MT, Domingo JLJJop, methods t. Assessing anxiety in C57BL/6J mice: a pharmacological characterization of the open-field and light/dark tests2014;69(2):108-14.
62. Prut L, Belzung CJEjop. The open field as a paradigm to measure the effects of drugs on anxiety-like behaviors: a review2003;463(1-3):3-33.
63. Chaouloff F, Durand M, Mormède PJBbr. Anxiety-and activity-related effects of diazepam and chlordiazepoxide in the rat light/dark and dark/light tests1997;85(1):27-35.
64. Fadok JP, Krabbe S, Markovic M, Courtin J, Xu C, Massi L, Botta P, Bylund K, Muller C, Kovacevic A, Tovote P, Luthi A. A competitive inhibitory circuit for selection of active and passive fear responses. Nature. 2017;542(7639):96-100. Epub 2017/01/25. doi: 10.1038/nature21047. PubMed PMID: 28117439.
65. Seo C, Guru A, Jin M, Ito B, Sleezer BJ, Ho Y-Y, Wang E, Boada C, Krupa NA, Kullakanda DSJS. Intense threat switches dorsal raphe serotonin neurons to a paradoxical operational mode2019;363(6426):538-42.
66. Le May MV, Hume C, Sabatier N, Schele E, Bake T, Bergstrom U, Menzies J, Dickson SL. Activation of the rat hypothalamic supramammillary nucleus by food anticipation, food restriction or ghrelin administration. J Neuroendocrinol. 2019;31(7):e12676. Epub 2018/12/24. doi: 10.1111/jne.12676. PubMed PMID: 30580497.
67. Vogel H, Wolf S, Rabasa C, Rodriguez-Pacheco F, Babaei CS, Stober F, Goldschmidt J, DiMarchi RD, Finan B, Tschop MH, Dickson SL, Schurmann A, Skibicka KP. GLP-1 and estrogen conjugate acts in the supramammillary nucleus to reduce food-reward and body weight. Neuropharmacology. 2016;110(Pt A):396-406. Epub 2016/08/09. doi: 10.1016/j.neuropharm.2016.07.039. PubMed PMID: 27496691.
68. Cryan JF, Valentino RJ, Lucki I. Assessing substrates underlying the behavioral effects of antidepressants using the modified rat forced swimming test. Neurosci Biobehav Rev. 2005;29(4-5):547-69. Epub 2005/05/17. doi: 10.1016/j.neubiorev.2005.03.008. PubMed PMID: 15893822.
69. Knoll AT, Carlezon Jr WAJBr. Dynorphin, stress, and depression2010;1314:56-73.
70. Ebner K, Singewald NJCOiBS. Individual differences in stress susceptibility and stress inhibitory mechanisms2017;14:54-64.

71. Chen S, He L, Huang AJY, Boehringer R, Robert V, Wintzer ME, Polygalov D, Weitemier AZ, Tao Y, Gu M, Middleton SJ, Namiki K, Hama H, Therreau L, Chevaleyre V, Hioki H, Miyawaki A, Piskorowski RA, McHugh TJ. A hypothalamic novelty signal modulates hippocampal memory. Nature. 2020;586(7828):270-4. Epub 2020/10/02. doi: 10.1038/s41586-020-2771-1. PubMed PMID: 32999460.
72. Andalman AS, Burns VM, Lovett-Barron M, Broxton M, Poole B, Yang SJ, Grosenick L, Lerner TN, Chen R, Benster T, Mourrain P, Levoy M, Rajan K, Deisseroth K. Neuronal Dynamics Regulating Brain and Behavioral State Transitions. Cell. 2019;177(4):970-85 e20. Epub 2019/04/30. doi: 10.1016/j.cell.2019.02.037. PubMed PMID: 31031000; PMCID: PMC6726130.
73. Berton O, Covington HE, 3rd, Ebner K, Tsankova NM, Carle TL, Ulery P, Bhonsle A, Barrot M, Krishnan V, Singewald GM, Singewald N, Birnbaum S, Neve RL, Nestler EJ. Induction of deltaFosB in the periaqueductal gray by stress promotes active coping responses. Neuron. 2007;55(2):289-300. Epub 2007/07/21. doi: 10.1016/j.neuron.2007.06.033. PubMed PMID: 17640529.
74. Tovote P, Esposito MS, Botta P, Chaudun F, Fadok JP, Markovic M, Wolff SB, Ramakrishnan C, Fenno L, Deisseroth K, Herry C, Arber S, Luthi A. Midbrain circuits for defensive behaviour. Nature. 2016;534(7606):206-12. Epub 2016/06/10. doi: 10.1038/nature17996. PubMed PMID: 27279213.
75. Keay KA, Bandler R. Parallel circuits mediating distinct emotional coping reactions to different types of stress. Neurosci Biobehav Rev. 2001;25(7-8):669-78. Epub 2002/01/22. doi: 10.1016/s0149-7634(01)00049-5. PubMed PMID: 11801292.
76. Lee A, Mathuru AS, Teh C, Kibat C, Korzh V, Penney TB, Jesuthasan S. The habenula prevents helpless behavior in larval zebrafish. Curr Biol. 2010;20(24):2211-6. Epub 2010/12/15. doi: 10.1016/j.cub.2010.11.025. PubMed PMID: 21145744.
77. Li B, Piriz J, Mirrione M, Chung C, Proulx CD, Schulz D, Henn F, Malinow R. Synaptic potentiation onto habenula neurons in the learned helplessness model of depression. Nature. 2011;470(7335):535-9. Epub 2011/02/26. doi: 10.1038/nature09742. PubMed PMID: 21350486; PMCID: PMC3285101.
78. Keay KA, Bandler R. Parallel circuits mediating distinct emotional coping reactions to different types of stress. Neurosci Biobehav R. 2001;25(7-8):669-78. doi: Pii S0149-7634(01)00049-5

Unsp 0149-7634/02/$

Doi 10.1016/S0149-7634(01)00049-5. PubMed PMID: WOS:000173861100011.
79. Shang C, Liu Z, Chen Z, Shi Y, Wang Q, Liu S, Li D, Cao P. BRAIN CIRCUITS. A parvalbumin-positive excitatory visual pathway to trigger fear responses in mice. Science. 2015;348(6242):1472-7. Epub 2015/06/27. doi: 10.1126/science.aaa8694. PubMed PMID: 26113723.
80. Molendijk ML, de Kloet ER. Immobility in the forced swim test is adaptive and does not reflect depression. Psychoneuroendocrino. 2015;62:389-91. doi: 10.1016/j.psyneuen.2015.08.028. PubMed PMID: WOS:000365062900044.
81. Swanson LW. The projections of the ventral tegmental area and adjacent regions: a combined fluorescent retrograde tracer and immunofluorescence study in the rat. Brain Res Bull. 1982;9(1-6):321-53. Epub 1982/07/01. doi: 10.1016/0361-9230(82)90145-9. PubMed PMID: 6816390.
82. Barbano MF, Wang HL, Zhang S, Miranda-Barrientos J, Estrin DJ, Figueroa-Gonzalez A, Liu B, Barker DJ, Morales M. VTA Glutamatergic Neurons Mediate Innate Defensive Behaviors. Neuron. 2020;107(2):368-82 e8. Epub 2020/05/23. doi: 10.1016/j.neuron.2020.04.024. PubMed PMID: 32442399; PMCID: PMC7381361.
83. Root DH, Mejias-Aponte CA, Qi J, Morales M. Role of glutamatergic projections from ventral tegmental area to lateral habenula in aversive conditioning. J Neurosci. 2014;34(42):13906-10. Epub 2014/10/17. doi: 10.1523/JNEUROSCI.2029-14.2014. PubMed PMID: 25319687; PMCID: PMC4198536.
84. Qi J, Zhang S, Wang HL, Barker DJ, Miranda-Barrientos J, Morales M. VTA glutamatergic inputs to nucleus accumbens drive aversion by acting on GABAergic interneurons. Nat Neurosci. 2016;19(5):725-33. Epub 2016/03/29. doi: 10.1038/nn.4281. PubMed PMID: 27019014; PMCID: PMC4846550.

85. Wang W, Schuette PJ, Nagai J, Tobias BC, Cuccovia VRFM, Ji S, de Lima MAX, La-Vu MQ, Maesta-Pereira S, Chakerian M, Leonard SJ, Lin L, Severino AL, Cahill CM, Canteras NS, Khakh BS, Kao JC, Adhikari A. Coordination of escape and spatial navigation circuits orchestrates versatile flight from threats. Neuron. 2021;109(11):1848-60 e8. Epub 2021/04/17. doi: 10.1016/j.neuron.2021.03.033. PubMed PMID: 33861942; PMCID: PMC8178241.
86. Wang W, Schuette PJ, La-Vu MQ, Torossian A, Tobias BC, Ceko M, Kragel PA, Reis FM, Ji S, Sehgal M, Maesta-Pereira S, Chakerian M, Silva AJ, Canteras NS, Wager T, Kao JC, Adhikari A. Dorsal premammillary projection to periaqueductal gray controls escape vigor from innate and conditioned threats. Elife. 2021;10. Epub 2021/09/02. doi: 10.7554/eLife.69178. PubMed PMID: 34468312; PMCID: PMC8457830.
87. Markham CM, Blanchard DC, Canteras NS, Cuyno CD, Blanchard RJ. Modulation of predatory odor processing following lesions to the dorsal premammillary nucleus. Neurosci Lett. 2004;372(1-2):22-6. Epub 2004/11/09. doi: 10.1016/j.neulet.2004.09.006. PubMed PMID: 15531081.
88. Vong L, Ye C, Yang Z, Choi B, Chua S, Jr., Lowell BB. Leptin action on GABAergic neurons prevents obesity and reduces inhibitory tone to POMC neurons. Neuron. 2011;71(1):142-54. Epub 2011/07/13. doi: 10.1016/j.neuron.2011.05.028. PubMed PMID: 21745644; PMCID: PMC3134797.
89. McCall JG, Al-Hasani R, Siuda ER, Hong DY, Norris AJ, Ford CP, Bruchas MR. CRH Engagement of the Locus Coeruleus Noradrenergic System Mediates Stress-Induced Anxiety. Neuron. 2015;87(3):605-20. doi: 10.1016/j.neuron.2015.07.002. PubMed PMID: WOS:000361145000013.
90. Sparta DR, Stamatakis AM, Phillips JL, Hovelso N, van Zessen R, Stuber GD. Construction of implantable optical fibers for long-term optogenetic manipulation of neural circuits. Nat Protoc. 2011;7(1):12-23. Epub 2011/12/14. doi: 10.1038/nprot.2011.413. PubMed PMID: 22157972; PMCID: PMC8647635.
91. Fenno LE, Mattis J, Ramakrishnan C, Hyun M, Lee SY, He M, Tucciarone J, Selimbeyoglu A, Berndt A, Grosenick L, Zalocusky KA, Bernstein H, Swanson H, Perry C, Diester I, Boyce FM, Bass CE, Neve R, Huang ZJ, Deisseroth K. Targeting cells with single vectors using multiple-feature Boolean logic. Nat Methods. 2014;11(7):763-72. Epub 2014/06/09. doi: 10.1038/nmeth.2996. PubMed PMID: 24908100; PMCID: PMC4085277.
92. Paxinos G, Franklin KB. Paxinos and Franklin's the mouse brain in stereotaxic coordinates: Academic press; 2019.
93. Porsolt RD, Bertin A, Blavet N, Deniel M, Jalfre M. Immobility induced by forced swimming in rats: effects of agents which modify central catecholamine and serotonin activity. Eur J Pharmacol. 1979;57(2-3):201-10. Epub 1979/08/01. PubMed PMID: 488159.
94. Martianova E, Aronson S, Proulx CD. Multi-Fiber Photometry to Record Neural Activity in Freely-Moving Animals. J Vis Exp. 2019(152). Epub 2019/11/05. doi: 10.3791/60278. PubMed PMID: 31680685.
95. Parker KE, Pedersen CE, Gomez AM, Spangler SM, Walicki MC, Feng SY, Stewart SL, Otis JM, Al-Hasani R, McCall JG, Sakers K, Bhatti DL, Copits BA, Gereau RW, Jhou T, Kash TJ, Dougherty JD, Stuber GD, Bruchas MR. A Paranigral VTA Nociceptin Circuit that Constrains Motivation for Reward. Cell. 2019;178(3):653-71 e19. Epub 2019/07/28. doi: 10.1016/j.cell.2019.06.034. PubMed PMID: 31348890; PMCID: PMC7001890.
96. Stamatakis AM, Stuber GD. Activation of lateral habenula inputs to the ventral midbrain promotes behavioral avoidance. Nat Neurosci. 2012;15(8):1105-7. Epub 2012/06/26. doi: 10.1038/nn.3145. PubMed PMID: 22729176; PMCID: PMC3411914.
97. Luskin AT, Bhatti DL, Mulvey B, Pedersen CE, Girven KS, Oden-Brunson H, Kimbell K, Blackburn T, Sawyer A, Gereau RWt, Dougherty JD, Bruchas MR. Extended amygdala-parabrachial circuits alter threat assessment and regulate feeding. Sci Adv. 2021;7(9). Epub 2021/02/28. doi: 10.1126/sciadv.abd3666. PubMed PMID: 33637526; PMCID: PMC7909877.

98. Richardson NR, Roberts DC. Progressive ratio schedules in drug self-administration studies in rats: a method to evaluate reinforcing efficacy. J Neurosci Methods. 1996;66(1):1-11. Epub 1996/05/01. doi: 10.1016/0165-0270(95)00153-0. PubMed PMID: 8794935.